

# **POLITECNICO DI TORINO**

Corso di Laurea Magistrale in Ingegneria Energetica e Nucleare



## **Experimental investigation of limestone dissolution and the effect of ultrasonic power by means of a stepwise titration method.**

### **Relatori**

prof. Massimo Santarelli  
prof. Tapio Westerlund  
prof. Cataldo De Blasio

### **Candidato**

Donatella Sinatra

Anno Accademico 2017/18



## Contents

List of Figures .....	ii
List of Tables .....	v
<b>1 Introduction.....</b>	<b>1</b>
1.1 Aim and structure of the thesis.....	4
<b>2 Theoretical background .....</b>	<b>5</b>
2.1 Geology and analyzed samples.....	5
2.2 Principles of Wet Flue Gas Desulfurization .....	8
<b>3 Modeling.....</b>	<b>13</b>
3.1 Mass transfer and kinetic modeling.....	14
3.2 Solid-liquid dynamics .....	18
3.3 Particle size distribution and specific surface area .....	19
3.4 Experimental procedure .....	23
<b>4 Results and discussion .....</b>	<b>27</b>
4.1 pH curves .....	27
4.2 Specific surface area and particle size distribution .....	32
4.3 Limestone consumption .....	36
<b>5 Scale-up study .....</b>	<b>41</b>
5.1 Power consumption for the agitation of the reaction tank.....	41
5.2 Scaling-up criteria.....	43
<b>Conclusions.....</b>	<b>46</b>
<b>Notation .....</b>	<b>47</b>
<b>Bibliografy.....</b>	<b>49</b>
<b>Appendices.....</b>	<b>55</b>

# List of Figures

Figure 1: Sector share of sulfur oxides emissions (EEA, 2014).....	2
Figure 2: Parainen small sample on the left and Wolica small sample on the right (Carletti et al., 2016). .....	7
Figure 3: Schematic representation of a wet FGD scrubber (Kitto & Stultz, 2005).....	10
Figure 4: Cumulative particle size distribution measured by laser diffraction for Parainen samples large size fraction and small size fraction.....	20
Figure 5: Probability density functions measured by laser diffraction for Parainen large size fraction and small size fraction.....	21
Figure 6: Experimental set-up.....	23
Figure 7: Screen of the Mastersizer software before the addition of the sample: it can be observed that the obscuration bar (left upper part of the screen) is 0%.....	25
Figure 8: Screen of the Mastersizer software the sample was added to the solution: it can be observed that the obscuration bar is now in the right range.....	25
Figure 9: . The pH as a function of time, for the large size fraction of the Wolica sample. ....	28
Figure 10 pH evolution in time for Wolica large fraction with (right) and without (left) the use of ultrasounds.....	31
Figure 11 pH evolution in time for Wolica small fraction with (right) and without (left) the use of ultrasounds.....	31
Figure 12 pH evolution in time for Parainen large fraction with (right) and without (left) the use of ultrasounds.....	32
Figure 13 pH evolution in time for Parainen small fraction with (right) and without (left) the use of ultrasounds.....	32

Figure 14: The Total Surface Area for all the tested samples evaluated by laser diffractometry measures without the use of the ultrasounds (left) and with the use of ultrasounds (right).  
.....33

Figure 15: PSD specific surface areas, SSA from PSD, and specific surface areas measured by the mean diameter, SSA from mean dp, before and after reaction for the Wolica large and small size fractions, without (left) and with (right) the use of ultrasounds. ....34

Figure 16: PSD specific surface areas, SSA from PSD, and specific surface areas measured by the mean diameter, SSA from mean dp, before and after reaction for the Parainen large and small size fractions, without (left) and with (right) the use of ultrasounds. ....34

Figure 17: Cumulative PSD (left) , probability density function (right) for Wolica small size fraction using the ultrasounds. ....35

Figure 18: Cumulative PSD (left) , probability density function (right) for Wolica small size fraction. ....35

Figure 19: Cumulative PSD (left) , probability density function (right) for Wolica large size fraction. ....36

Figure 20: Cumulative PSD (left) , probability density function (right) for Parainen large size fraction. ....36

Figure 21: Cumulative PSD (left) , probability density function (right) for Parainen small size fraction. ....36

Figure 22: The pH as a function of time for the small size fraction and large fraction of the Wolica sample (left) and Parainen sample (right), using the ultrasounds. ....37

Figure 23: Hydronium ions concentration as a function of time for the small size fraction and large fraction of the Wolica sample, without the ultrasounds (left) and using the ultrasounds (right). ....37

Figure 24: Hydronium ions concentration as a function of time for the small size fraction and large fraction of the Parainen sample, without the ultrasounds (left) and using the ultrasounds (right). ....38

Figure 25: Hydronium ions concentration time evolution from experimental pH measurements (dotted line) and from the theoretical hydronium ions content (solid line) for

Wolica large size fraction, without the use of ultrasounds (left) and with the use of ultrasounds (right). .....38

Figure 26: Power needed for the stirring of the large scale reactor for the three different scale-up criteria. ....45

# List of Tables

Table 1: Potential reduction of SO <sub>x</sub> control technologies (Franco & Diaz, 2009).....	3
Table 2: Sample type, density, CaCO <sub>3</sub> content and composition (wt%).....	7
Table 3: FGD processes. ....	8
Table 4: First records of the pH meter. ....	29
Table 5: Measures of the SSA. ....	29
Table 6: Limestone consumption data sheet. ....	30
Table 7: Limestone consumption. ....	39

# 1 Introduction

The industrialization has had a strong impact on the environment and the resulting global energy demand has increased considerably in the last century. Statistics found that the global energy mix in 2013 was dominated by the fossil fuels, such as coal, oil and gas, that still make up to 81% of the total primary energy supply (IEA, 2015) and according to the World Energy Outlook (WEO), the energy generated from fossil fuels is expected to cover up to 84% of the energy demand.

Sulfur dioxide ( $\text{SO}_2$ ) and sulfur trioxide ( $\text{SO}_3$ ), or generally speaking sulfur oxides ( $\text{SO}_x$ ), are emitted from the combustion or the oxidation of fossil fuels like oil and coal that have traces of sulfur as impurity.  $\text{SO}_x$  represent the major atmospheric sulfur-based pollutants since they contribute to acid deposition that strongly modifies soil and water quality. Acid deposition effects on the environment include: alterations on natural water systems such as lakes and rivers, damages to crops and forests, damages to buildings.  $\text{SO}_x$  emissions can worsen asthma conditions, reduce lungs functionality, inflame the respiratory tract and since they contribute to the formation of particulate aerosols in the atmosphere, they are also indirectly linked to human health. Several progresses in the reduction of the  $\text{SO}_x$  emissions have been globally achieved. Regulations on emissions limits have been adopted for the last 30 years in most of the industrialized countries and in some developing countries. Among the EEA-33 members (28 EU members countries together with Iceland, Liechtenstein, Norway, Switzerland and Turkey), the  $\text{SO}_x$  emissions diminished by the 74% during 1990-2011. In 2011 the main source of  $\text{SO}_x$  emissions came from the 'Energy production and distribution' sector (58% of

total emissions), followed by the 'Energy use in industry' sector (20%) and from the 'Commercial, institutional and households' sector (15%) (EEA, 2014).

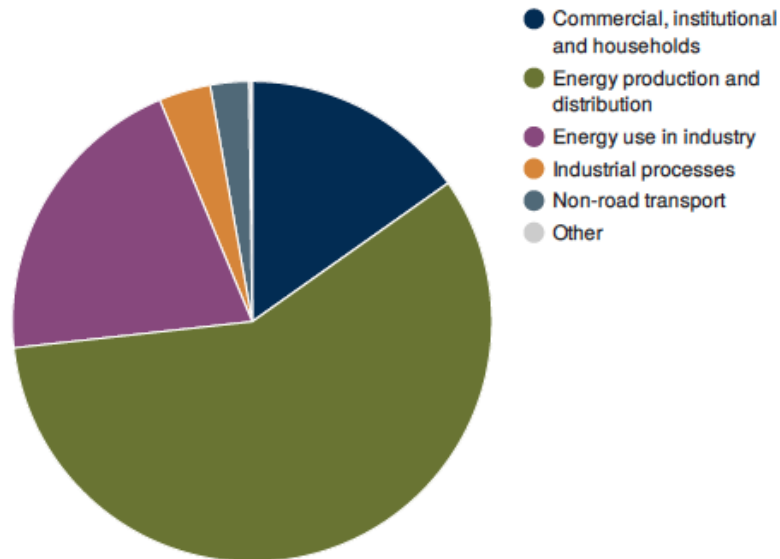


**Figure 1:** Sector share of sulfur oxides emissions (EEA, 2014)

The main contribution in the  $SO_x$  reduction were in the 'Waste' sector (84%), 'Energy production and distribution' (76%), 'Energy use in industry' (72%) and 'Commercial, institutional and households' (64%). The 'Energy production and distribution' sector makes up to the largest share, contributing to the 65% in terms of absolute reduction. The reduction in the emissions from electricity generation was achieved thanks to different factors such as efficiency improvements, increased share of nuclear and renewable energy, fuel-switching from high-sulfur to low-sulfur fuels such as natural gas and mostly due to flue gas desulfurization (Sloss, 2011).

According to the World Energy Outlook (WEO), the trends in fossil fuels utilization will not decrease and even if worldwide research into other energy sources have been developed in the last 40 years, mainly due to the uncertain future regarding the fossil fuel reservoirs, the global energy market will still depend on fossil fuels in the near future (Shafiee & Topal, 2009). An example could be the coal: it's an abundant widely spread energy resource, available at a lower and stable cost among the other fossil fuels. Even if it can't be considered

a long-term solution for the energy issue, coal plays a key-role in the energy generation for the developing countries and also for the others. Nowadays, 23% of the global primary energy comes from coal and roughly the 36% of the world's electricity is produced from coal. China, USA, India, Germany, Australia still use it as main fuel. Even if cleaner fuel remains the best option for Europe and other countries, there is still the necessity to use coal as an energy source to meet both increasing electricity demand and plant retirements. The increasing energy demands of the developing countries combined with the necessity of the greenhouse gas emissions are the challenging responsibility of present and future energy policies. The success of 'clean coal technologies' characterized by good thermodynamic performance combined with the control of pollutant emissions, explains the perspective of coal as an energy source.

To meet the requirements of the SO<sub>2</sub> reduction regulations, many existing power plants have adopted flue gas desulfurization (FGD) technologies.

Different technologic solutions regarding the FGD have been proved to be effective and to have sulphur dioxide removal efficiency even higher than 95%. Since the power consumed in the scrubber operation can reach the 2% of the total installed power in a plant, necessary research and improvements in the reactor design and optimization are still necessary. A variety of FGD technologies are available nowadays, but Wet Flue Gas Desulfurization scrubbers are the most used for plants using coal as fuel.

**Table 1:** Potential reduction of SO<sub>x</sub> control technologies (Franco & Diaz, 2009).

<b>Control techniques</b>	<b>SO reduction potential (%)</b>
Pre-combustion removal: physical cleaning	30 - 50 % removal, inorganic sulfur
Chemical and biological cleaning	90 % removal, organic sulfur
Combustion configuration: fluid bed	80 - 98 %
Post-combustion removal: WFGD	
In situ sulfur capture: dry sorbent injection (DSI)	50%

## 1.1 Aim and structure of the thesis

Limestone dissolution has been regarded as one most relevant factor in sulfur removal in Wet Flue Gas Desulfurization applications. The aim of this work is to give a characterization in terms of Particle Size Distribution and Specific Surface Area available for the reaction of two types of sample from Finland using ultrasounds power. This aim has been pursued through the simulation of the acidic environment of the WFGD tank by using hydrochloric acid. This has been done in order to obtain the limestone consumption to be used for a comparison in term of removal efficiency among the different samples.

This thesis is structured into five chapters. Chapter 2 presents the theoretical background of limestone dissolution and Wet Flue Gas Desulfurization. Chapter 3 gives a description of the modeling of the kinetics, mass transfer and the solid-liquid dynamics, a description of the characterization methods used and the related experimental procedure. Chapter 4 gives the results and the discussion of this experimental work. Chapter 5 presents a scaling-up model to evaluate the power required for the stirring of the reaction tank.

# 2 Theoretical background

There are several technologies for the SO<sub>2</sub> emissions reduction from the exhaust gas produced in the power plants nowadays: they allow a power plant to meet the emission standards and its impact on the environment. These technologies include: fuel switching to low-sulfur coal or using of blended-fuel, which are convenient methods, since the plant doesn't need to change the boiler or to purchase a desulfurization system; coal preparation, that involves the improvement of the quality in the production phase; boiler modernisation, which means that at the end of its life-cycle, the boiler is repaired instead of been replaced; technology change from coal to natural gas; flue gas desulfurization (FGD) (Kaminski, 2003). Among all the previously mentioned methods, FGD is the widest applied method for sulfur emissions reduction. The most used FGD technology in the energy sector is absorption of sulfur dioxide in a limestone slurry, known as wet scrubbing (Kiil, Michelsen, & Dam-Johansen, 1998). According to Kaminski they have been estimated to account for the 84% of the market share of the total capacity or even higher than the 90% (Hrastel, Gerbec, & Stergaršek, 2007).

## 2.1 Geology and analyzed samples

Most of the installed FGD applications have a calcium-based sorbent, so the slurry could be made of limestone or lime. Limestone (mostly made of CaCO<sub>3</sub>) is one the most common sorbents used in WFGD applications thanks to its low price and the possibility to exploit the produced gypsum as by-product.(F.J.Gutiérrez Ortiz, F.Vidal, P.Ollero, L.Salvador, V.Cortés, 2006).

Calcium carbonate rocks are sedimentary rocks very abundant on Earth, containing mineral carbonates like calcite ( $\text{CaCO}_3$ ), dolomite ( $\text{Mg}(\text{CaCO}_3)_2$ ), aragonite, siderite ( $\text{FeCO}_3$ ) and magnesite ( $\text{MgCO}_3$ ). In particular,  $\text{CaCO}_3$  is the most plentiful sediment in the oceans, constituting roughly the 10% of sediments (Al Omari, Rashid, Qinna, Jaber, & Badwan, 2016). Chemical and biochemical processes contribute to the formation of carbonates. Chemical processes can be the direct precipitation of salts in a solution or the variations of some parameters like the concentration, the pH and the temperature of the solution. Biochemical processes occur with the presence of living organisms. The majority of these processes takes place in seawater environments. After the deposition, the carbonate structure can be greatly modified by the chemical and physical processes of diagenesis. The diagenesis of carbonate rocks includes different processes and it takes place near the marine surface and meteoric environments. Some of this process are: cementation, dissolution, dolomitization, compaction, neomorphism and microbial micritization. Carbonate minerals, aragonite, calcite and dolomite are mostly involved by carbonate diagenesis but other minerals as quartz, clay minerals, iron oxide sulphides can also be involved.

Calcium carbonate rocks can be classified by different parameters, such as the magnesium content or the matrix content, such as those of Folk (1959,1962) and Dunham (1962)(Al Omari et al., 2016). Another way to classify carbonate rocks is by using the terminology of the crystallography, which is used to describe the symmetry, structure and shape of mineral crystals. According to the type of symmetry possessed by a mineral species, the species can be classified as a member of one out of six crystal systems and one out of thirty-two crystal classes. In addition, there are two main system architectures: the hexagonal and the trigonal system. Hence, considering the architecture of the crystal structure, vaterite has hexagonal structure, aragonite has a rhomboid one while calcite has a trigonal structure.

Limestone can be composed of different minerals, but it is mostly made of calcite, such as the samples used for this work. In the calcite group there are minerals characterized by a general formula of  $\text{ACO}_3$ , where A is a metal ion like calcium, iron, magnesium, nickel and others. The purity of limestone is determined by the calcium carbonate content or CaO content and a sample with of  $\text{CaCO}_3 > 98.5\%$  or  $\text{CaO} > 55.2$  has high purity limestone content.

Experiments were conducted on two different types of limestone, both quite pure in  $\text{CaCO}_3$  content, but they belong to different geological backgrounds and proveniences and this reflects on their morphology and reactivity.

The samples used were Wolica and Parainen, both characterized by two size fractions with 74–125  $\mu\text{m}$  and 212–250  $\mu\text{m}$  mesh sizes. The Parainen sample comes from Finland and it is a metamorphic limestone from the Proterozoic age. The Wolica sample comes from Poland and it is a sedimentary limestone from the Jurassic age. The total  $\text{CaCO}_3$  composition, the samples density and the bulk composition (wt%) of the metal oxides contained in the samples are presented in Table 2.

**Table 2:** Sample type, density,  $\text{CaCO}_3$  content and composition (wt%).

Sample	$\rho$ (kg/m <sup>3</sup> )	$\text{CaCO}_3$ %	CaO wt%	$\text{Al}_2\text{O}_3$ wt%	SiO wt%	MgO wt%
Parainen	2720	98.5	54.5	0.13	0.5	0.59
Wolica	2703	99.1	55.2	0.01	0.05	0.32

Some examples of the Scanning Electron Microscopy (SEM) images for the Wolica and the Parainen sample are shown in Figure 2.

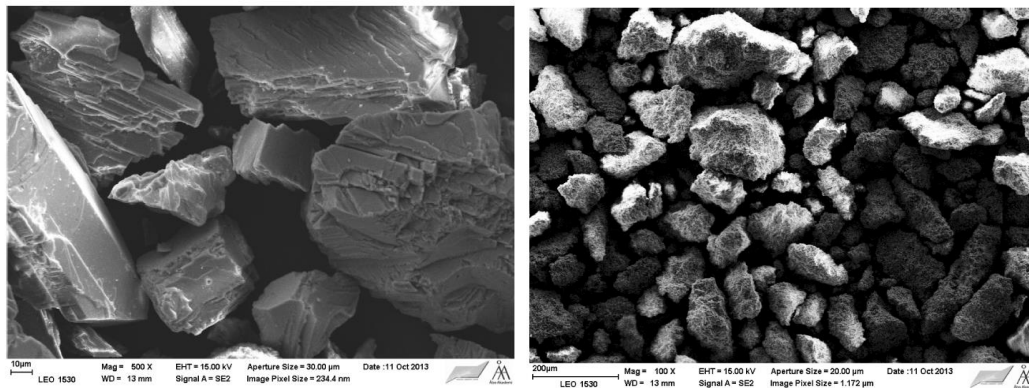


**Figure 2:** Parainen small sample on the left and Wolica small sample on the right (Carletti et al., 2016).

As mentioned previously, comparing the two samples, it can be easily noted that the two samples have a very different morphology. The Wolica sample seems to be less uniform than the Parainen one, but they both have a lot of surface irregularities, which means that both samples have a good amount of surface area available for the reaction, more than the same particles had a spherical surface, which is the assumption needed if the shrinking sphere model hypothesis is adopted (Levenspiel, 1999).

## 2.2 Principles of Wet Flue Gas Desulfurization

Wet Flue Gas (FGD) techniques consist of removing the SO<sub>2</sub> from the exhaust gases of the combustion using some sorbents.

FGD methods can be classified in two types, regenerable and once-through.

**Table 3:** FGD processes.

Flue Gas Desulfurization			
Once-through		Regenerable	
Wet	Dry	Wet	Dry
Limestone Forced Oxidation	Lime Spray Drying	Sodium Sulfit	Activated Carbon
Limestone Inhibited Oxidation	Furnace Sorbent Injection	Magnesium Oxide	
Jet Bubbling Reactor	LIFAC	Sodium Carbonate	
Lime	Economizer Sorbent Injection	Amine	
Magnesium-Enhanced Lime	Duct Sorbent Injection		
Dual Alkali	Duct Spray Drying		
Seawater	Circulating Fluidized Bed		
	Hypas Sorbent Injection		

The regenerable technology applications don't produce any waste, since a sorbent regeneration occurs and during this process the SO<sub>2</sub> leaves the sorbent. In once-through technologies, the SO<sub>2</sub> is trapped in the sorbent that must be disposed as a waste at the end of the FGD process or reused as a byproduct (as gypsum). Both processes can be named as

either wet or dry. In wet technologies flue gases leave the absorber saturated with water and there is a production of wet slurry. In dry processes the flue gases that leave the absorber are not saturated and dry waste is produced. Since the marginal use of regenerable FGD methods, once-through FGD methods currently represent the most common applications (Srivastava & Jozewicz, 2001). Wet FGD has been considered the most effective and the least expensive (Olausson, Wallin, & Bjerle, 1993), and in particular limestone-gypsum based wet technologies are the most used thanks to the high efficiency and reliability (Zhong et al., 2008). A representation of a counter-current WFGD scrubber is presented in Figure 3.

In these scrubbers the exhaust gas enters from the midsection of the tower where it is put in contact with the wet slurry, pumped by spray nozzles until it's reduced into fine droplets, then it is depleted of the SO<sub>2</sub> and finally leaves the absorber from the top saturated with water. The SO<sub>2</sub> dissolves in the slurry droplets and the slurry containing SO<sub>2</sub> goes in a reaction tank, where the lime or limestone particles of the slurry dissolve and the reaction with SO<sub>2</sub> continues. The slurry is recirculated to the higher part of the tower where it is sprayed into the entering flue gas. During this process, there is an accumulation of chloride ions in the process liquid because the hydrogen chloride inside the exhaust gas is also absorbed and neutralized with the reagents. The absorber liquor, which is the slurry that has already reacted with the flue gas, is collected on the bottom of the reaction tank where it is agitated to prevent settling. Fresh limestone or lime is added to the reaction tank to refill the limestone consumed. In this process the slurry is also aerated and then recirculated to the spray nozzles. Part of the slurry is retained to produce gypsum salts that are removed as sludge. This sludge is then separated from the liquor to be dewatered for the storage and the final disposal. The final gypsum byproduct can be disposed in a landfill or more conveniently, if the limestone content is under the 4 wt %, it can be sold (F.J.Gutiérrez Ortiz, F.Vidal, P.Ollero, L.Salvador, V.Cortés, 2006).

There are different design parameters that have an impact on the final SO<sub>2</sub> removal efficiency of WFGD systems and one of these is the liquid-to-gas (L/G) ratio, which is the quantity of liquid of recirculated slurry to inlet flue gas ratio. High value of L/G means that the flue gas is exposed to more absorbing liquor but also it means a higher consumed power. The sulfur removal efficiency can be improved by the addition of organic acids to the reaction tank:

since the slurry absorbs the acidic  $\text{SO}_2$ , these additives act like buffers to stabilize the pH of the slurry, so the solubility of  $\text{SO}_2$  in the slurry increases and the absorber can operate with a lower L/G ratio. Another advantage is that, since there is a lower pH, the rate of dissolution on limestone and the reagent utilization increases (Sargent & Lundy LLC, 2003). The most used organic acids are adipic, glycolic, formic, maleic and acrylic acids.

The organic acid needs to be replenished after the oxidative degradation in the absorber and to replace the part taken out in the moisture of the gypsum and in the wastewater.

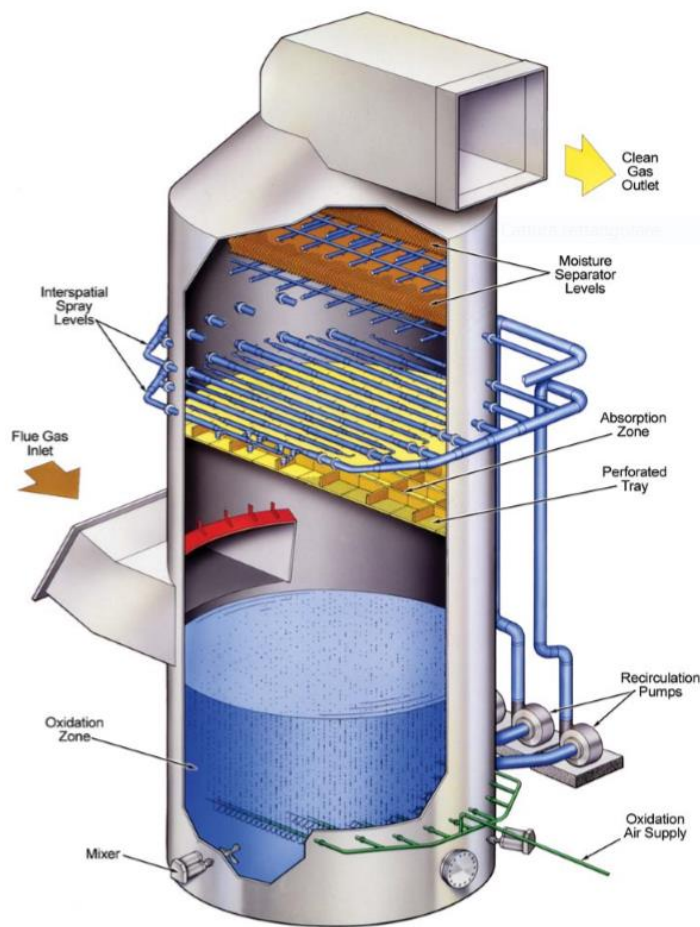


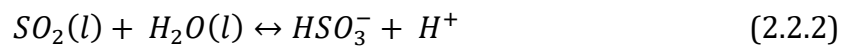
**Figure 3:** Schematic representation of a wet FGD scrubber (Kitto & Stultz, 2005).

A simplification of the main reactions occurring in limestone and lime-based reactors is the following (Roddy, 2010). In the gas-liquid contact zone of the absorber:

Dissolution of sulphur dioxide from the gaseous state into the liquid one



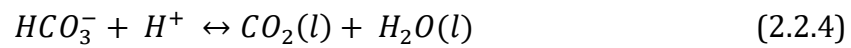
Hydrolysis of sulfur dioxide into hydrogen and bisulfur ions



The limestone dissolution resulting into calcium ions and bicarbonate



The acid-base neutralization



The stripping of the carbon dioxide

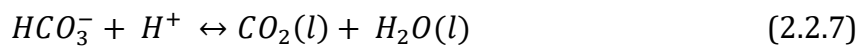


In the reaction tank of the scrubber the following reactions occur:

The limestone dissolution



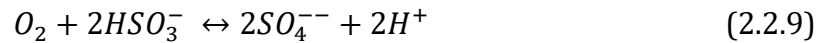
The acid-base neutralization



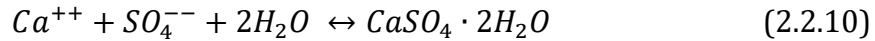
The stripping of the carbon dioxide



Sulfite oxidation



The crystallization of gypsum



The most used technology in the market is the limestone scrubber with forced oxidation (LSFO), so the overall chemical reaction in wet FGD with forced oxidation is,



In a LSFO droplets of water/limestone slurry are sprayed (Baukal, 2003) from the top while the flue gas inlet is in the bottom in a counter-flow layout. The SO<sub>x</sub> captured in the slurry is sent in a liquid/solid separator like a hydroclone.

The main advantages of this process:

- sulphur dioxides removal efficiency up to 98%;
- tested reliability;
- feasibility on different coals;
- the absorbent material has a low cost;
- forced oxidation allows greater use of limestone than other systems;
- the final product can be easily disposed and the gypsum produced has a market value;
- LSFO represents an easier retrofit than natural oxidation.

The process disadvantages:

- high energy consumptions to achieve high removal efficiencies;
- the necessity to use expensive anti-corrosion material in the absorption tower and the recycle tank;
- heating of the exhaust gas.

# 3 Modeling

Limestone is one of the most common material in the earth and it is widely used in several industrial sector therefore a large range of research within different fields has been carried out to the study of limestone dissolution. In the last 30 years this research field has been widely explored but the FGD systems still need to be improved. Some studies focused on the effect of some organic acids to improve the removal efficiency (Eden & Luckas, 1998), (Liu & Xiao, 2006), in particular the efficiency has improved from 83% to 90% using adipic acid (Frandsen, Kiil, & Johnsson, 2001).

The limestone dissolution has been investigated through the shrinking-sphere model by several authors (Shih, Lin, & Shiau, 2000), (Altun, 2014), (Siagi & Mbarawa, 2009). According to this model, the particles are considered to have smooth surfaces and a spherical geometry and the surface of the reaction, which is a sphere, diminishes as the conversion proceeds (Levenspiel, 1999).

Some studies have used different geometries and experimental conditions to investigate the diffusion of limestone in acidic solutions: fixed bed dissolution (Lancia, Musmarra, & Pepe, 1997), step-wise titration method (Ahlbeck, Engman, Fältén, & Vihma, 1993), free-drift method (Plummer, Wigley, & Parkhurs, 1978), rotating discs (Bjerle & Rochelle, 1984), (Sjöberg & Rickard, 1985),(Lund, Fogler, & McCune, 1977) and parallel planes (Williams et al., 1970).

The limestone dissolution has been considered as a first order reaction (Ahlbeck et al., 1993), (Williams et al., 1970), (Plummer et al., 1978). Several studies have found that the dissolution rate depends on the degree of agitation and that it is controlled by mass transfer (Sjöberg & Rickard, 1983), (Pepe, 2001).

As what can be observed from all the previous consideration, it's not straightforward to find mathematical model to describe the limestone dissolution in acidic conditions. The

phenomenon is influenced by different experimental conditions and it is also subjected to several uncertainties. and because of the complexity of the hydrodynamics of the system.

### 3.1 Mass transfer and kinetic modeling

A large number of industrial processes involve solid-liquid reactions, especially in the chemicals production field such as dissolution of solids and precipitation. One parameter that must be taken into account is that the rate of the heterogeneous reaction depends on the available surface area rather than the solid concentration, but the determination of the surface area is not so straightforward. Moreover, pressure, temperature and just a few other parameters can be directly measured, so the complexity of these systems is the main reason why the studies on solid-liquid reactions use indirect methods to estimate the surface area. When dealing with solid-fluid reactions where the mass transfer rates and chemical reactions rates on the solid surface are comparable, both mass transfer and chemical reactions need to be considered and the rates of both of them must be compared. Therefore, basing on the ratio between the chemical reaction rates and the mass transfer rate, it can be determined if there is diffusion control or reaction control or a combination of both.

The Damköhler number,  $Da$  is a dimensionless quantity defined as the ratio between the reaction rate constant and the mass transfer coefficient. If the reaction is a first order reaction,

$$Da = \frac{k_r}{k_l} \quad (3.1.1)$$

so when  $Da$  is a very small number, the concentration of the species at the surface is close to zero; if  $Da$  has a large value the concentration is more or less equal to the bulk concentration. In this work, both mass transfer and chemical reaction are taken onto account.

In the case of spherical particles, the mass transfer coefficients can be determined through semi-empirical equations that take into account molecular diffusion and forced convection. The Sherwood equation can be written as (J. Welty, Gregory L. Rorrer, 1970),

$$Sh = Sh_0 + CRe^a Sc^{1/3} \quad (3.1.2)$$

where  $C$  and  $a$  are the constants to be evaluated (J. Welty, Gregory L. Rorrer, 1970) and  $Sh_0$  can be approximated to the value 2 in the case of a spherical particle immersed in a stagnant fluid.

The Froessling equation can be used for the case of the terminal velocity-slip theory,

$$Sh = 2 + 0.44Re^{1/2} Sc^{0.38} \quad (3.1.3)$$

Otherwise, for the case of Kolmogoroff's theory of local isotropic turbulence,

$$Sh = 2 + 0.6Re^{1/2} Sc^{1/3} \quad (3.1.4)$$

The Froessling equation is adopted when the settling velocity is greater than 0.0005 m/s. Considering also the Stokes regime, the Sherwood equation becomes (Bird, Stewart, & Lightfoot, 2002),

$$Sh = 2 + 0.991(ReSc)^{1/3} \quad (3.1.5)$$

The Sherwood number can be obtained from,

$$Sh = \frac{k_l d_p}{D_j} \quad (3.1.6)$$

with  $k_l$  is the mass transfer coefficient,  $d_p$  is the particle diameter and  $D_j$  is the diffusivity of the  $j$  species.

The Schmidt number can be obtained as,

$$Sc = \frac{\nu}{D_j} \quad (3.1.7)$$

where  $\nu$  is the kinematic viscosity of the fluid.

When dealing with mass transfer in solid-liquid systems, the literature gives two main theories to calculate the Reynolds number for the particles: the Kolmogoroff theory of local isotropic turbulence and the terminal velocity-slip theory.

From the Kolmogoroff's theory,

$$Re_p = \left( \frac{\varepsilon d_p^4}{\nu^3} \right)^{1/3} \quad (3.1.8)$$

where  $\varepsilon$  is the mean dissipated energy. The Reynolds number obtained from the theory of terminal velocity-slip is,

$$Re_p = \frac{u_t d_p}{\nu} \quad (3.1.9)$$

The Reynolds number for the vessel is obtained from,

$$Re_v = \frac{N D_s^2}{\nu} \quad (3.1.10)$$

with  $N$  is the stirring speed and  $D_s$  is the stirrer diameter.

A model that gives a good approximation of the kinetic of reactions of particles immersed in a fluid is the shrinking-core model. According to this model, the reaction initially occurs at the external part of the particle towards the inner part and then progressively, as the reaction moves forward, the core of unreacted material shrinks, leaving behind converted and inert material (Levenspiel, 1999).

When dealing with kinetic modeling it's important to determine how some parameters affect the reaction and one of the most crucial is the effect of the temperature on the reaction rate. The Arrhenius theory gave one of the earliest description of the effect of the temperature on the rate constant,

$$k_r = k_I e^{\left(\frac{-E_a}{R_g T}\right)} \quad (3.1.11)$$

where  $k_I$  is the pre-exponential factor,  $E_a$  is the activation energy and  $R_g$  is the universal gas constant.

Both the exponential factor and the activation energy can be considered not dependent from the temperature.

The literature proposes modifications of the original Arrhenius equation, such as the following,

$$k_r = k_I e^{\frac{-E_a}{R_g} \left(\frac{1}{T} - \frac{1}{T_{mean}}\right)} \quad (3.1.12)$$

where the correlation between the pre-exponential factor and the activation energy is minimized.

## 3.2 Solid-liquid dynamics

In the study of solid-liquid dynamics like suspension systems, one parameter that has to be taken into account and that can be considered as a constant value is the settling velocity of a particle in a fluid. Once a particle has reached its settling velocity, this velocity can be calculated applying the balance of forces acting on the particle itself. The forces are: the drag force, the weight and the buoyancy. The drag force can be evaluated using the Schiller and Naumann equation,

$$C_D = \frac{24}{Re_p} (1 + 0.15Re_p^{0.687}) \quad (3.2.1)$$

where  $C_D$  is the drag coefficient.

The expression of the settling velocity,

$$u_t = \sqrt{\frac{4d_p g(\rho_s - \rho_l)}{3\rho_l C_D}} \quad (3.2.2)$$

where  $d_p$  is the mean diameter of the particle,  $g$  is the gravity acceleration,  $\rho_s$  and  $\rho_l$  are respectively the solid and the liquid phase densities.

A modified equation to obtain the settling velocity has been proposed,

$$u_t = \sqrt{\frac{4d_p g(\rho_s - \rho_l)}{3\rho_l C_D (1 - \varphi)^{-1.65}}} \quad (3.2.3)$$

where  $\varphi$  is the volumetric fraction of solids.

In the applications involving agitation of solid particles in a liquid, it's fundamental to determine the minimum stirring speed at which all the particles are suspended: this

condition is called complete suspension. In this condition, the maximum of the surface area of the particles is exposed and available to the bulk for the chemical reaction (Paul, Atiemo-Obeng, & Kresta, 2004). The literature presents several experimental methods for the estimation of  $N_{js}$  but one of the most used is the visual observation of the off-bottom suspension of the solid particles (Ibrahim, Jasnin, Wong, & Baker, 2012). The following equation has been obtained in the research work of Zwietering (1958) that covered the largest range of variables and it has been massively applied,

$$N_{js} = S \left( g \frac{\rho_s - \rho_l}{\rho_l} \right)^{0.45} (d_p)^{0.2} (X_{mass})^{0.13} (\nu)^{0.1} (D_s)^{-0.85} \quad (3.2.4)$$

where  $S$  is a dimensionless parameter depending on the system geometry,  $X_{mass}$  is the fraction (%) of solid in suspension,  $D_s$  is the impeller diameter,  $\nu$  is the kinematic viscosity.

### 3.3 Particle size distribution and specific surface area

Wet Flue Gas Desulfurization processes are directly affected by the size distribution of the particles since they influence the dissolution rates of limestone (Toprac & Rochelle, 1982; Ukawa, Takashina, Shinoda, & Shimizu, 1993).

The determination of the particle size which is actually referred to the particle diameter is not a straightforward process and it needs a basic introduction. The basis of this topic is related to the concept of the equivalent diameter, which is the diameter of a hypothetical particle that is the equivalent of the considered object concerning a certain property, for instance the volume. Obviously it is hardly probable that the particle has a spherical shape, so another aspect to be considered is the particle shape.

Currently different types of particle size analysis equipment are used and each of them may provide equivalent diameters based on different properties, such as projected area, mesh size, projected area, surface area, etc. Since the large amount of different options that have to

be considered, the most appropriate technique to represent the particle size data depends on the final use of the data. In mass transfer calculations, for example, the equivalent spherical diameter by surface area per unit volume is the best option (Holdich, 2002).

Another aspect to take into account is that the same powder may be represented with different particle size functions. The cumulative function is built by taking the total quantity of particles and convert it to a fractional amount for every size range. An illustration of the volume based PSD measured by laser diffraction (Malvern Mastersizer 3000) for the Parainen fractions is shown in Figure 4.

Focusing on the large fraction: all the particles are smaller than 665  $\mu\text{m}$ , therefore 100% or 1.0 as size fraction of the particles is smaller than this size. Approximately, the 60% is smaller than 309  $\mu\text{m}$ . There are not particles smaller than 111  $\mu\text{m}$ , so the cumulative number undersize is zero. Moreover, comparing the curves of the two fractions, it is clear that the large fraction is composed of larger particles, since its cumulative is on the right part of the plot.

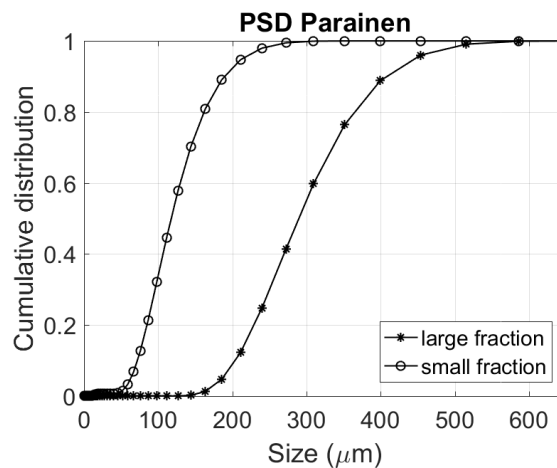


**Figure 4:** Cumulative particle size distribution measured by laser diffraction for Parainen samples large size fraction and small size fraction.

It is also possible to represent the particle size distribution based on the frequency curve with a bell shaped curve, which are the probability density functions (PDF). These curves shown in Figure 5 can be used to build the cumulative curves of Figure 4.

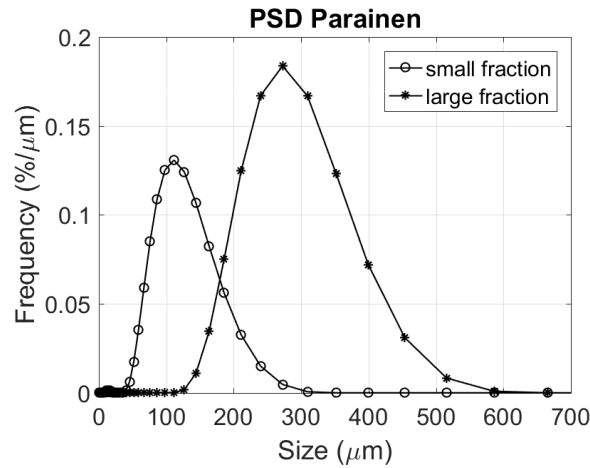


**Figure 5:** Probability density functions measured by laser diffraction for Parainen large size fraction and small size fraction.

The distributions in Figure 5 are normalized: the total area under the curve is unity. By the normalization, i.e. dividing by the micron range, the two curves are related: the cumulative is the integral form of the PDF and the PDF is the differential of the cumulative.

Now it is necessary to introduce a parameter related to fluid flow problems and reactivity, i.e. the specific surface area per unit mass (SSA). The SI units are  $\text{m}^2/\text{kg}$ . The SSA can be referred to a full size distribution by considering the total surface area (TSA) divided by the mass of the distribution,

$$SSA = \frac{6 \sum \frac{V_i}{d_i}}{\rho \sum V_i} \quad (3.3.1)$$

where  $V_i$  is the relative diameter in size class  $i$  characterized by a mean diameter of  $d_i$  and  $\rho$  is the particle density.

It can be also introduced another concept to represent the particle size distribution: the equivalent spherical diameter also known as Sauter Mean Diameter,

$$D[3,2] = \frac{\sum V_i}{\sum \frac{V_i}{d_i}} \quad (3.3.2)$$

This parameter is the diameter of a spherical particle that has the same SSA as the distribution. Adopting this concept, it is possible to rewrite the previous expression of the SSA in the following way,

$$SSA = \frac{6}{\rho D_{[3,2]}} \quad (3.3.3)$$

In limestone-water slurry applications laser diffraction is the way to evaluate the PSD and in particular, this technique employs low angle laser light scattering to estimate the volumetric distribution of the sample.

When the light strikes a solid particle, it is partially absorbed, reflected, diffracted and transmitted. Under the assumption of spherical and optically homogeneous particles, the laser diffraction method reads the scattering patterns of the diffracted light, using the Mie or Fraunhofer theories.

The Fraunhofer theory considers that the particles are opaque or that there is no refraction, and that the wavelength of the light used in the measure is smaller than the particles. The Mie Theory takes into account also the refraction but it has the drawback of the necessity to know both the real and the imaginary absorption parts of the refractive index. The Fraunhofer approximation can be used when the particles are larger than 25  $\mu\text{m}$ , since commonly a laser beam employed has a wavelength of 0.63  $\mu\text{m}$ . In fact when a laser beam passes through a suspension of particles, the diffraction angle is inversely proportional to the particle diameter. On the contrary modern lasers that use the Mie theory method can evaluate particle sizes in the 0.1-2000  $\mu\text{m}$  range (Rhodes, 2008). The Fraunhofer theory has been applied in this work, measuring the PSD by laser diffraction.

### 3.4 Experimental procedure

The experimental procedure adopted in this work is called free drift method (Plummer et al., 1978), with the modification of the step-by-step titration method (Ahlbeck, Engman, Fältén, & Vihma, 1995).

In the experiments that use the free drift method the dissolution of limestone is approached by adding a strong acid to a solution made of the solid sample and water and letting the reaction proceed until the near equilibrium, while the step-by-step modification implies the addition of acid more than once.

The experimental set-up is shown in Figure 6 consisting of a laser diffraction particle size analyzer for wet dispersion connected to a computer logger 1, a glass reactor, a scale, a pH electrode, a temperature control device, a pH meter connected to a computer logger 2.

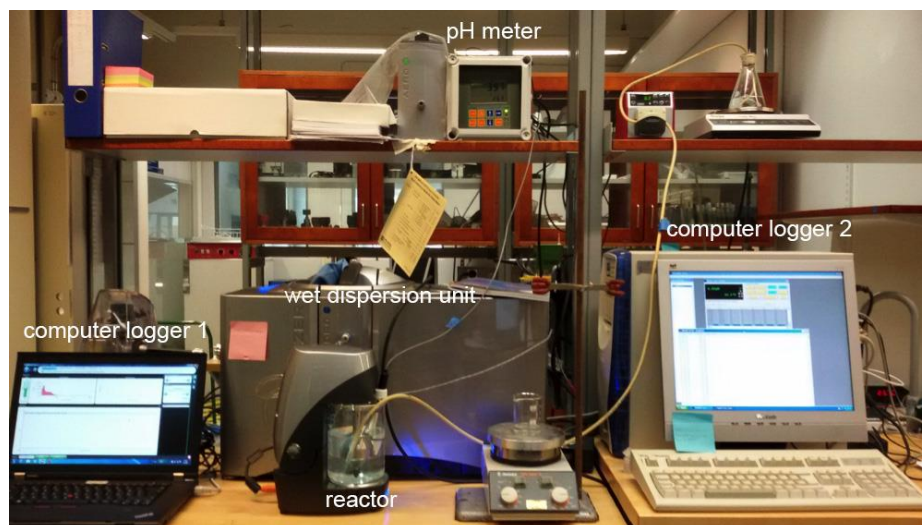


**Figure 6:** Experimental set-up.

The pH meter was calibrated before each measurement using pH buffers of 4.01 and 7.01 at room temperature. All the experiments were performed adding hydrochloric acid into a dispersion containing limestone and the reaction was allowed to proceed until equilibrium is attained. The values of pH and temperature were recorded by means of the software

HI92500 which allowed recordings every 5 s. The reaction was performed in 0.5 L of de-ionized water where different amounts of the solid samples (varying between 0.8 up to 2 g) were let react with 1 mL of HCl.

The particle size distribution of the samples was measured with laser diffraction (Malvern Mastersizer 3000) by applying the Fraunhofer theory.

All the experiments were performed with constant stirring speed (2300 rpm).

The procedure consisted of adding the solid sample to the reactor containing 0.5 L of de-ionized water: the mass of the samples ranged between 0.8 g and 3 g, depending on the type of sample and whether or not the ultrasounds were used. The first stage was to measure the background, which corresponds to the solution of the liquid dispersant, in this case the water, and the limestone.

The laser needs a certain amount of particles well dispersed to give statistically relevant measurements, therefore the right amount of the mass sample was chosen checking if the obscuration bar of the software was in the range between 2-24%. The obscuration is a parameter related to the laser and it helps to determine the mass of the sample when it is added to the dispersant. It can be defined as the amount of laser light lost as a result of the addition of the sample into the analyser beam. Usually the action of the ultrasounds with the same amount of sample, will cause the obscuration to rise more even than 40%: in fact, the ultrasound tends to destroy particles faster, so to achieve a good dispersion a smaller mass of the same sample was needed and typically the experiments were shorter. In Figure 7 and Figure 8 it can be observed how the obscuration of the Mastersizer software before adding the sample was 0% and after adding the sample was finally in the range.

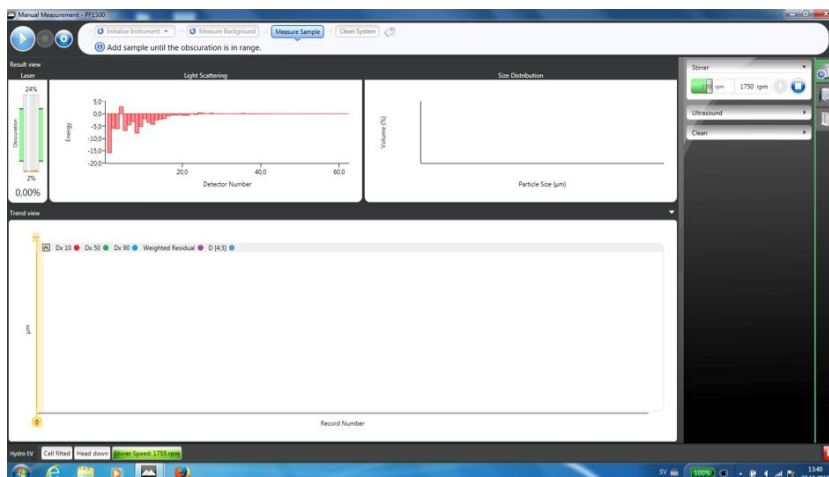


**Figure 7:** Screen of the Mastersizer software before the addition of the sample: it can be observed that the obscuration bar (left upper part of the screen) is 0%.

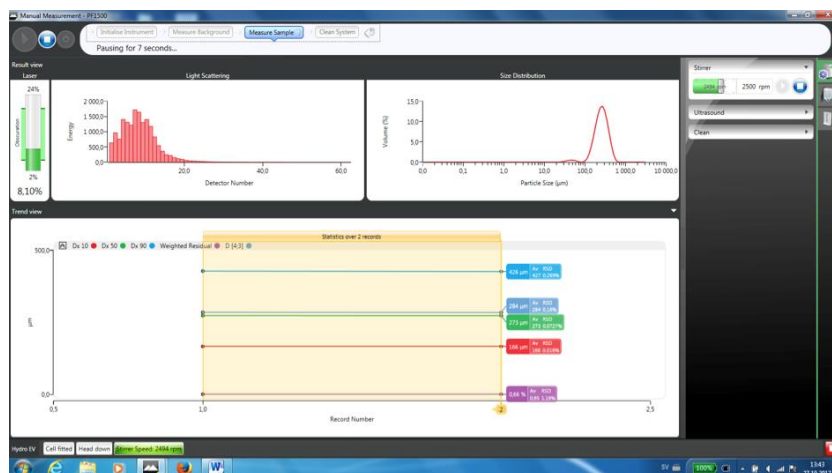


**Figure 8:** Screen of the Mastersizer software the sample was added to the solution: it can be observed that the obscuration bar is now in the right range.

The first three/ four measurements were dedicated to the record of the specific surface area (SSA) and the particle size distribution (PSD) of the sample.

After the background measures, the next step was the addition of a 1mL of HCl (1 mol/L): the pH meter recorded a sudden drop of the pH, from 6-7 to 3-3.5. The software kept on record SSA and PSD measures of the solution.

Then, when the dispersion reached the pH it got before the addition of HCl or when the increase rate of the pH increased slowly, the procedure was repeated: 1mL of acid was added, while the pH was being continuously measured and the SSA measures took place again.

This procedure was repeated up to five or seven or ten times, depending on the use of ultrasounds and the type of samples. At the end of every single experiment the pH records were saved and exported from the HI92500 software, while the SSA and PSD measurements were saved and exported from Mastersizer software.

# 4 Results and discussion

The pH measures have been used to calculate the amount of consumed limestone, the SSA records to calculate the total surface area and the particles mean diameter.

All the experiments related to a single sample have been repeated three times, with and without the use of the ultrasounds. The reason of it lies in the complexity of the study of limestone dissolution, which is still challenging nowadays. Therefore a case was chosen to be represented.

## 4.1 pH curves

All the experiments performed on limestone samples carried out similar behaviours regarding the trend of the pH in time, with small differences depending on the different parameters between one experiment and the other. The pH evolution in time of the Wolica Large is shown in Figure 9: it will be the only one explained in detail because all the other plots have similar trends and they don't diverge very much and all the procedures involved in the calculations are the same for all the experiments.

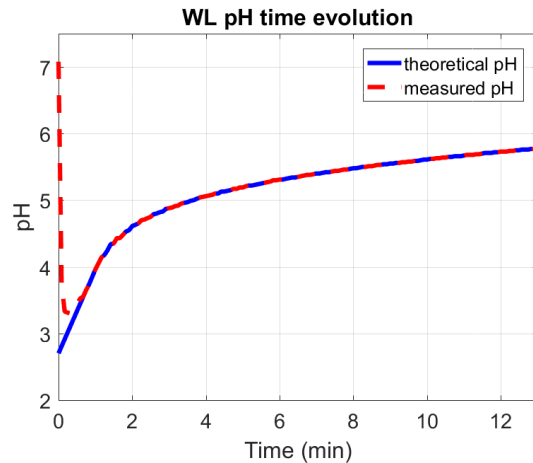


**Figure 9:** . The pH as a function of time, for the large size fraction of the Wolica sample.

Two different curves are shown in the Figure 9. The red dashed curve corresponds to the pH measurements actually recorded by the pH meter: the value of 7 in the pH scale corresponds to the pH value of the solution of water and limestone (the background solution), just before adding the HCl. This solution is characterized by a small alkalinity.

The blue curve corresponds to an interpolated curve obtained by the theoretical pH which, right after the addition of HCl, is slightly different from the recorded pH. The explanation is that the pH meter is fixed in a certain position of the reaction tank, so at the beginning of the experiment the measurements are affected by a non-instant homogeneous distribution of the HCl. Therefore the pH meter measurement gives a slightly higher value of the pH with respect to the theoretical one that can be obtained directly by the definition of pH related to the presence of  $H^+$  ions in the solution.

This has been done because the frequency of the measurements of the pH meter and the particle size analyzer were different: the Table 4 shows the first records of the pH meter, while in the Table 5 there are all the SSA measurements of the first step and it is clear that the time of the pH measures and the SSA measures are rarely coincident. Therefore, only for the first measure right after the adding of the acid, an interpolation was performed, since the exact value of the pH of the solution was needed.

**Table 4:** First records of the pH meter.

First measure_t1		
time	time	pH
	[s]	
16:20:49	0	7,08
16:20:54	5	3,75
16:20:59	10	3,33
16:21:04	15	3,31
16:21:09	20	3,3
16:21:14	25	3,35
16:21:19	30	3,43
16:21:24	35	3,52
16:21:29	40	3,55
16:21:34	45	3,65
16:21:39	50	3,74
16:21:44	55	3,85
16:21:49	60	3,96
16:21:54	65	4,05
16:21:59	70	4,14
16:22:04	75	4,18
16:22:09	80	4,25

**Table 5:** Measures of the SSA.

Step1 measurements		
measure	time	SSA
		[m <sup>2</sup> /g]
t1	16:21:32	9,2384586
t2	16:23:48	9,3174523
t3	16:24:31	9,3028347
t4	16:25:14	9,323893
t5	16:25:57	9,3458478
t6	16:26:41	9,3075216
t7	16:27:24	9,35799
t8	16:28:07	9,3447289
t9	16:28:50	9,3538332
t10	16:29:33	9,3366497
t11	16:30:16	9,336958
t12	16:30:59	9,3802745
t13	16:31:43	9,3049622
t14	16:32:26	9,3619855

The theoretical pH was calculated by the definition of pH, taking into account all the H<sup>+</sup> ions of the solution, both from the water and the acid, and considering the actual volume of the solution. Once the theoretical pH was calculated, a simple interpolation curve of the second/third order between the theoretical pH and the first measure available of the pH meter was obtained in order to have the exact value of the pH of the first SSA measurement. The number of H<sup>+</sup> ions was again calculated to obtain the consumed HCl moles from the moment of the addition of the acid to the first SSA measurement. Considering the limestone dissolution reaction, one mole of HCl dissolves one mole of CaCO<sub>3</sub>, therefore the number of consumed limestone moles are the same of the consumed moles of HCl. In this way, the consumed mass of limestone was calculated, step by step, for all the measurements of every steps. Once obtained the remaining CaCO<sub>3</sub> in the solution, multiplying this value for the measured SSA, the TSA was finally obtained. One step of the data sheet of every experiment is presented in Table 6. A detailed explanation of all the calculations done in this phase and an example of the data sheet are reported in the appendix.

**Table 6:** Limestone consumption data sheet.

	time	bg pH	bg [H <sup>+</sup> ] mol in 1 l	actual bg H+ mol in 0.5 l	total H+ mol in 0.5 l	[H+] mol in 1 l	pH00	pH	[H+] mol in 1 l	total H+ mol in 0.5 l	consumed HCl [moles]	consumed CaCO <sub>3</sub> [moles]	consumed CaCO <sub>3</sub> [g]	remaining CaCO <sub>3</sub> [g]	SSA [cm <sup>2</sup> /g]	TSA [cm <sup>2</sup> ]
t1	16:21:32	7,08	8,32E-08	4,16E-08	1,00E-03	2,00E-03	2,70	3,63	2,32E-04	1,16E-04	8,84E-04	8,84E-04	0,0885	1,9171	92,38	177,11
t2	16:23:48							4,88	1,32E-05	6,59E-06	9,93E-04	9,93E-04	0,0994	1,9062	93,17	177,61
t3	16:24:31							5,00	1,00E-05	5,00E-06	9,95E-04	9,95E-04	0,0996	1,9060	93,03	177,31
t4	16:25:14							5,13	7,41E-06	3,71E-06	9,96E-04	9,96E-04	0,0997	1,9059	93,24	177,70
t5	16:25:57							5,21	6,17E-06	3,08E-06	9,97E-04	9,97E-04	0,0998	1,9058	93,46	178,11
t6	16:26:41							5,30	5,01E-06	2,51E-06	9,98E-04	9,98E-04	0,0998	1,9058	93,08	177,38
t7	16:27:24							5,36	4,37E-06	2,18E-06	9,98E-04	9,98E-04	0,0999	1,9057	93,58	178,34
t8	16:28:07							5,42	3,80E-06	1,90E-06	9,98E-04	9,98E-04	0,0999	1,9057	93,45	178,08
t9	16:28:50							5,48	3,31E-06	1,66E-06	9,98E-04	9,98E-04	0,0999	1,9057	93,54	178,25
t10	16:29:33							5,53	2,95E-06	1,48E-06	9,99E-04	9,99E-04	0,0999	1,9057	93,37	177,92
t11	16:30:16							5,57	2,69E-06	1,35E-06	9,99E-04	9,99E-04	0,1000	1,9056	93,37	177,93
t12	16:30:59							5,62	2,40E-06	1,20E-06	9,99E-04	9,99E-04	0,1000	1,9056	93,80	178,75
t13	16:31:43							5,66	2,19E-06	1,09E-06	9,99E-04	9,99E-04	0,1000	1,9056	93,05	177,32
t14	16:32:26							5,71	1,95E-06	9,75E-07	9,99E-04	9,99E-04	0,1000	1,9056	93,62	178,40

The pH time evolution for all the samples is presented in Figure 10, Figure 11, Figure 12 and Figure 13. The curves obtained by the direct measures of the pH meter and the curves calculated by the interpolation from the pH obtained by the actual number of  $H^+$  ions of the solution in the moment of the acid addition are both plotted.

It can be observed that the pH reaches an almost constant value faster for the smaller fractions, as Wolica and Parainen small, with respect to the larger fractions Wolica and Parainen Large. The same comparison can be done also with the experiments with the application of ultrasounds: as mentioned before, the action of ultrasounds tends to dissolve faster the limestone particles.

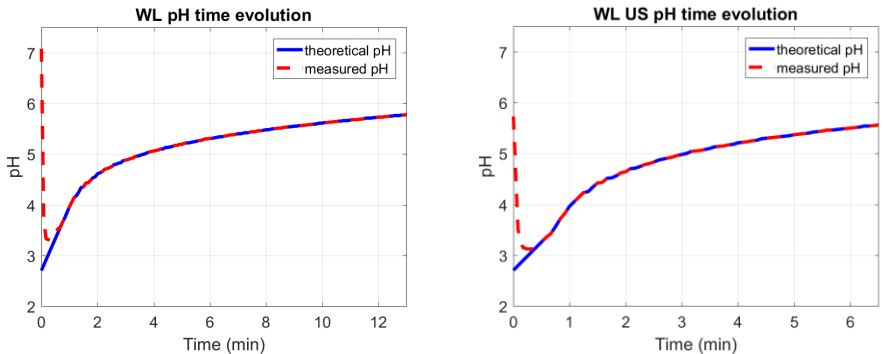


**Figure 10** pH evolution in time for Wolica large fraction with (right) and without (left) the use of ultrasounds.

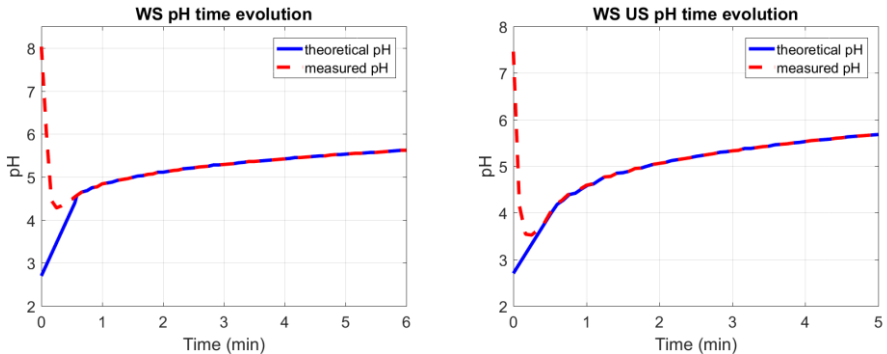


**Figure 11** pH evolution in time for Wolica small fraction with (right) and without (left) the use of ultrasounds.

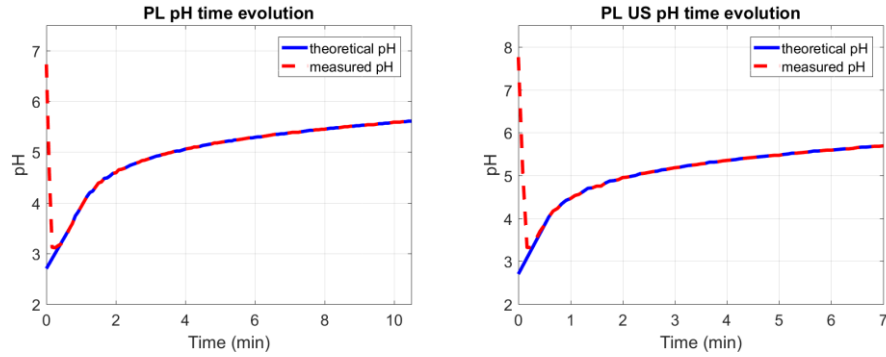


**Figure 12** pH evolution in time for Parainen large fraction with (right) and without (left) the use of ultrasounds.

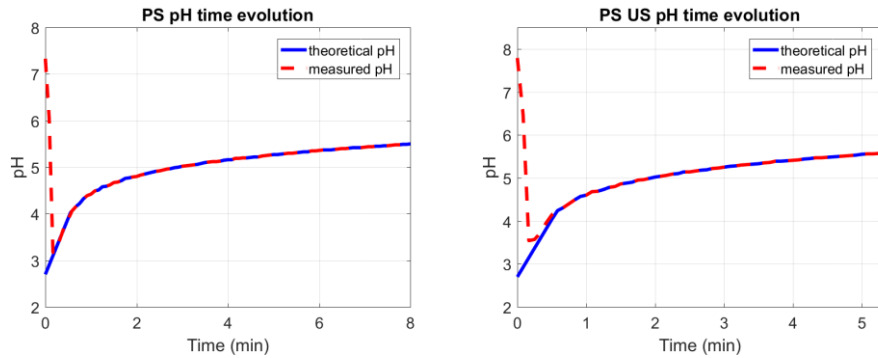


**Figure 13** pH evolution in time for Parainen small fraction with (right) and without (left) the use of ultrasounds.

## 4.2 Specific surface area and particle size distribution

As already mentioned previously, the specific surface area of the reaction was obtained from experimental measurements with laser diffractometry. These values change along with the evolution of the single experiment; despite this, it is possible that the Total Surface Area available for the reaction does not necessarily decrease during the course of the experiment, in fact sometimes the appearing of roughness in the particles surface or the formation of pits may increase the specific surface area. The main reason is that the particles may disintegrate, causing the enhancement of the surface valuable for the reaction (De Blasio et al., 2016). The Total Surface Area can be considered approximately constant for the large size fractions of the experiments performed without the use of the ultrasounds and for the Parainen large

fraction adopting the ultrasounds as the mass of the limestone is consumed, it slowly decreases for most of the titration steps, while it can sometimes increase if the presence of ruggedness on the surface of the reaction is more marked or after particles breaking. The TSA obtained by laser diffraction for all the samples and for all the steps is presented in Figure 14.

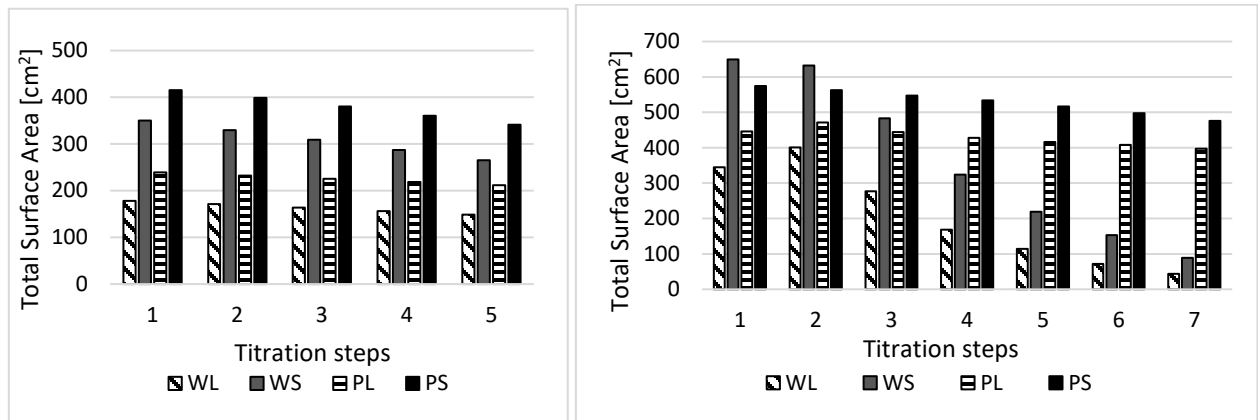


**Figure 14:** The Total Surface Area for all the tested samples evaluated by laser diffractometry measures without the use of the ultrasounds (left) and with the use of ultrasounds (right).

The SSA can be evaluated from the PSD measures of the surface area of a sphere having the same volume of the particle so it can be identified a class of particles characterized by the diameter of the equivalent sphere. The mean diameters of such spheres were calculated by fitting the cumulative distributions to Log-Normal probability density functions.

The specific surface area obtained from the PSD by the laser diffraction measurements were compared to the specific surface area calculated by the mean diameter.

The results are shown in Figure 15 and Figure 16 and for all the experiments performed without the ultrasounds, there are not any substantial differences between SSA from the mean diameter and SSA from PSD, even if the later are always slightly larger. However, for all the measurements performed with the use of the ultrasounds, the SSA obtained from PSD are larger than the others. In Figure 15 and Figure 16 the volume based PSD for the two samples and the for both size fractions is presented before the experiment and at the end of it.

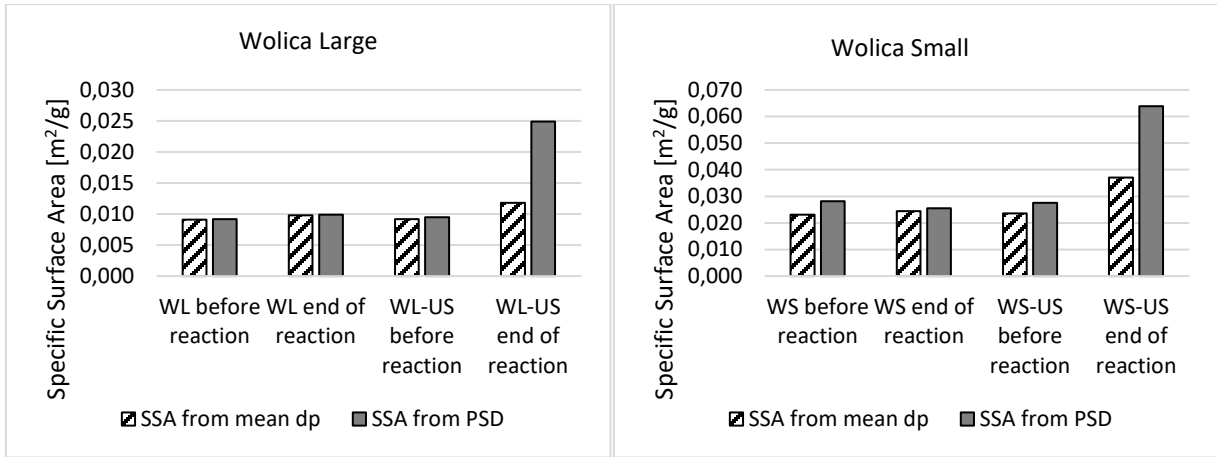


**Figure 15:** PSD specific surface areas, SSA from PSD, and specific surface areas measured by the mean diameter, SSA from mean dp, before and after reaction for the Wolica large and small size fractions, without (left) and with (right) the use of ultrasounds.

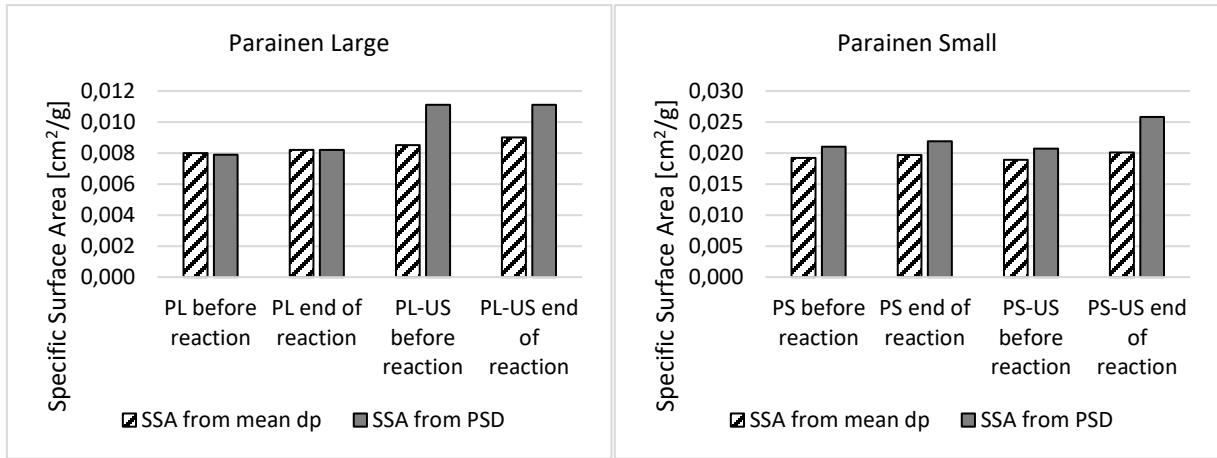


**Figure 16:** PSD specific surface areas, SSA from PSD, and specific surface areas measured by the mean diameter, SSA from mean dp, before and after reaction for the Parainen large and small size fractions, without (left) and with (right) the use of ultrasounds.

The PSD curves give information on how the particles size, so the particles diameter, changes during the reaction.

As the reaction proceeds, the size of the particles diminishes and this is shown in Figure 17. This result confirms the assumption adopted in literature of the shrinking-core model (Siagi & Mbarawa, 2009), (Shih et al., 2000), (Guelli U Souza, Santos, Ulson de Souza, & Vidal Barrero, 2010), (Altun, 2014), which considers the reduction of the size of the particles during the reaction.

The cumulative PSD for the small size fraction of the Wolica sample is presented in the plot on the left: the first curve on the right corresponds to a measurement of the background composed by the limestone sample and the water. The first step curve corresponds to the measure of the first addition of HCL and so on. It can be observed the decrease of the size particles during the course of the experiments by the shifting of the curves towards the left of the plot. The same behaviour can be seen also in the plot on the right, where the probability density function is shown.

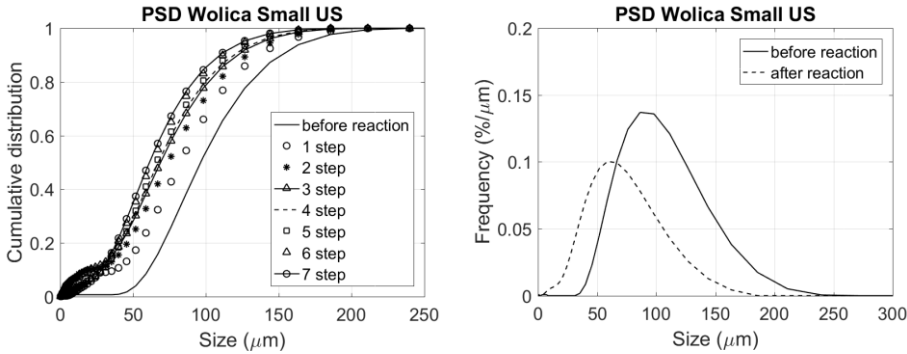


**Figure 17:** Cumulative PSD (left) , probability density function (right) for Wolica small size fraction using the ultrasounds.

Figure 18 shows the cumulative PSD of Wolica small fraction without the use of the ultrasounds: comparing this curve with the PSD of Figure 17, the effect of the ultrasounds is clear, since the latter PSD is wider than the other one, proving its stronger breaking down ability. The cumulative PSD for all the samples are presented in the next figures.

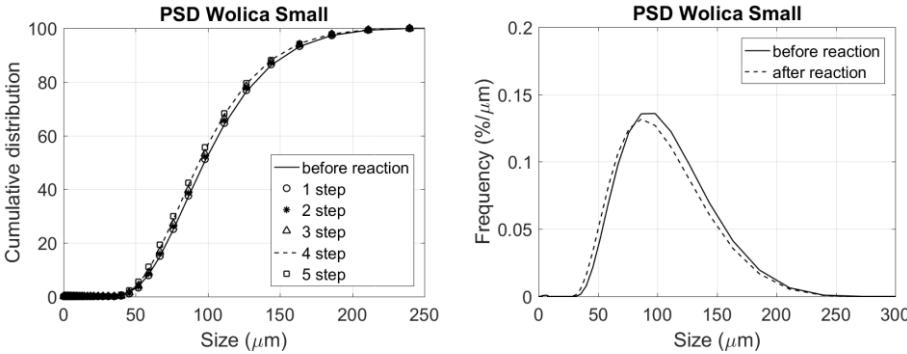


**Figure 18:** Cumulative PSD (left) , probability density function (right) for Wolica small size fraction.

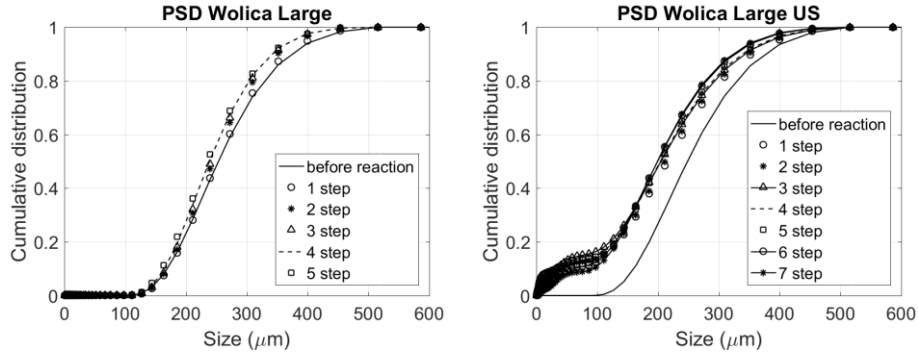


Figure 19: Cumulative PSD (left) , probability density function (right) for Wolica large size fraction.

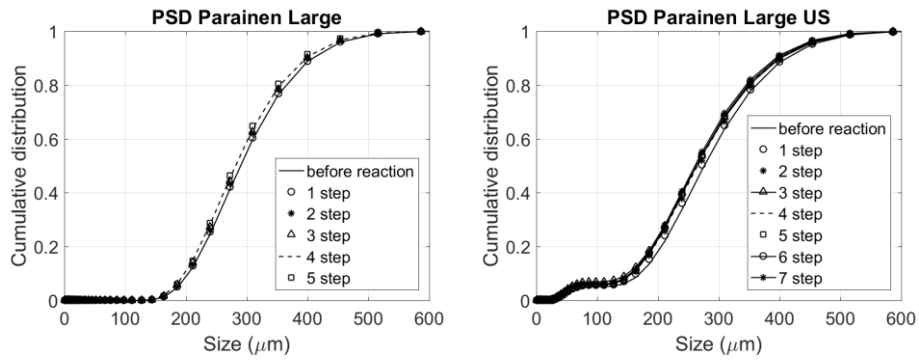


Figure 20: Cumulative PSD (left) , probability density function (right) for Parainen large size fraction.

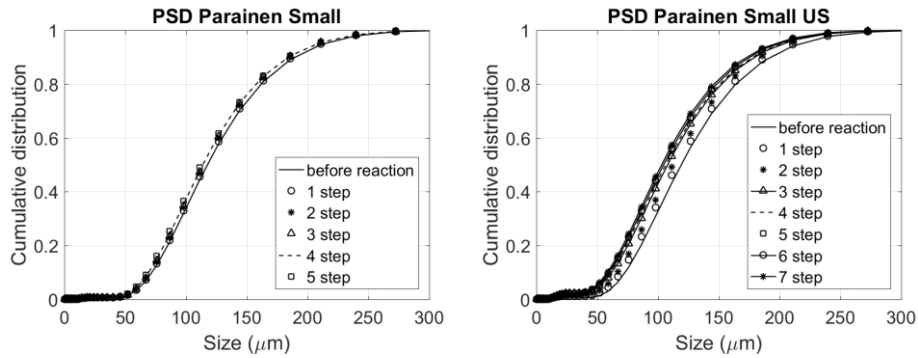
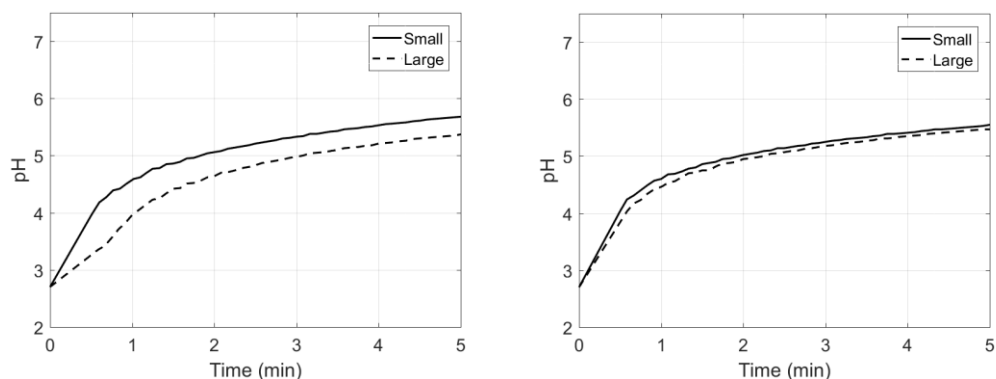


Figure 21: Cumulative PSD (left) , probability density function (right) for Parainen small size fraction.

### 4.3 Limestone consumption

The pH of the mixture was constantly measured to obtain the hydronium ions concentration in order to evaluate the limestone mass consumption.

In Figure 22 the pH evolution in time is presented for the small and large size fractions of the Wolica sample using the ultrasounds. It's possible to observe that the increase of the pH is related to the decrease of the hydronium ions concentration of the mixture (coming from both the water and the HCl), during the reaction. As expected, the reaction rate tends to slow down as the reaction proceeds (pH curve increase rate slows down), due to the progressive consumption of hydronium ions. The plot of Figure 22 displays that the small size fraction reacts faster than the large size fraction.



**Figure 22:** The pH as a function of time for the small size fraction and large fraction of the Wolica sample (left) and Parainen sample (right), using the ultrasounds.

A better representation of the hydronium ions consumption is realized when the evolution of the  $H^+$  ions concentration in time is plotted, and this is displayed in the following figures.

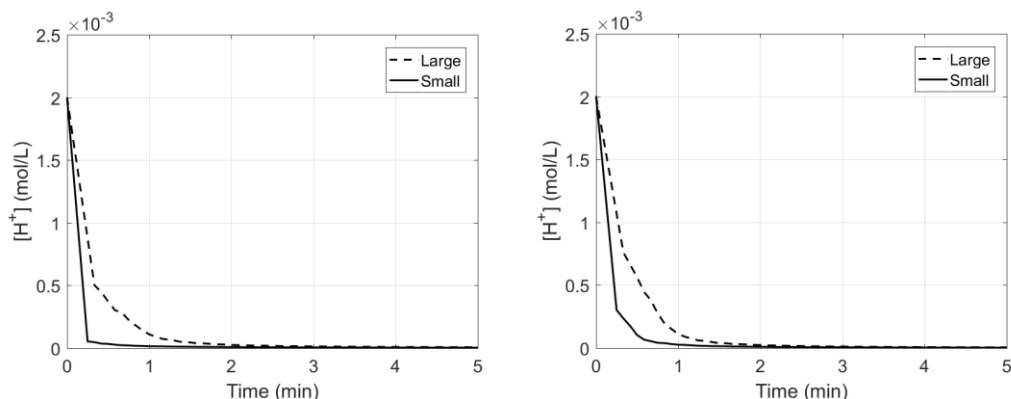


**Figure 23:** Hydronium ions concentration as a function of time for the small size fraction and large fraction of the Wolica sample, without the ultrasounds (left) and using the ultrasounds (right).

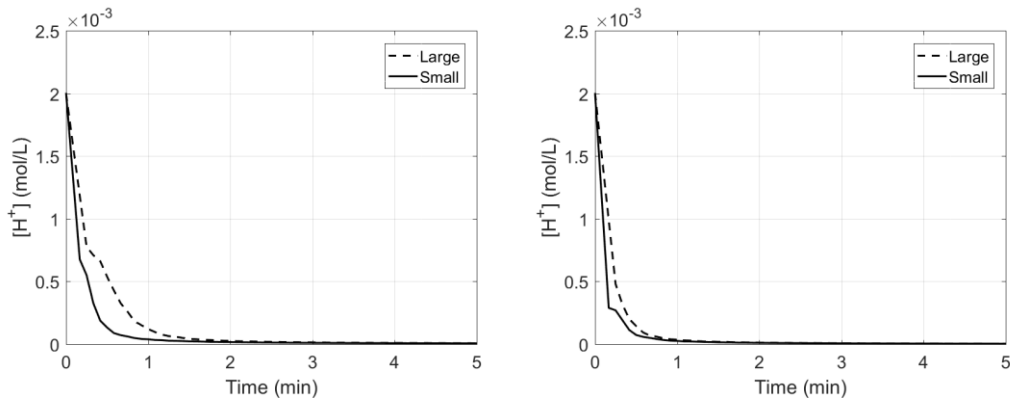


**Figure 24:** Hydronium ions concentration as a function of time for the small size fraction and large fraction of the Parainen sample, without the ultrasounds (left) and using the ultrasounds (right).

The hydronium ions concentration obtained by the pH measurements was used to calculate directly the amount of consumed limestone. Therefore, as explained previously in the first paragraph of this chapter, for the initial phase corresponding to the addition of the HCl, instead of using the measured pH, the hydronium ions concentration was calculated from the actual ions content coming from the water and the HCl. Both these curves are presented in Figure 25, just for the Wolica large size fraction sample, since the behaviour of the curves is similar for all the samples. The same explanation related the pH curves applies to the hydronium ions concentration: as expected the initial  $H^+$  ions concentration is the same for all the experiments and it is higher for the theoretical curves with respect to the experimental curve.

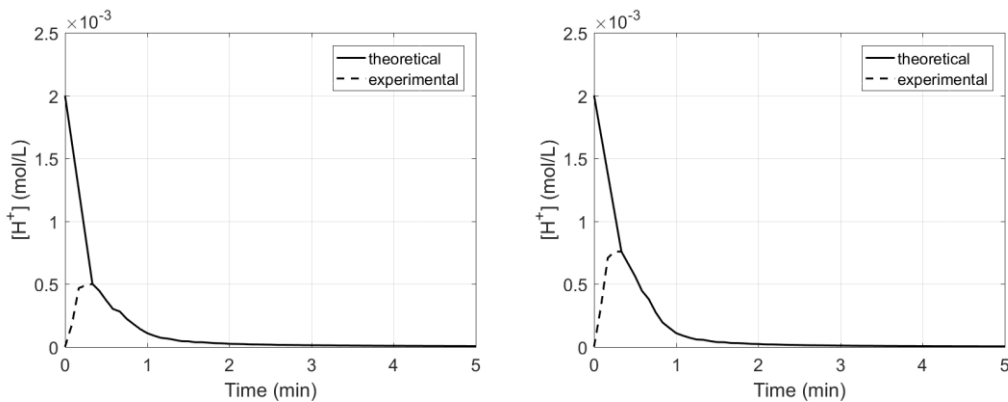


**Figure 25:** Hydronium ions concentration time evolution from experimental pH measurements (dotted line) and from the theoretical hydronium ions content (solid line) for Wolica large size fraction, without the use of ultrasounds (left) and with the use of ultrasounds (right).

The limestone consumed during the experiment was calculated directly from the H<sup>+</sup> ions content of the mixture at every measure with the assumption that in the limestone dissolution reaction one molecule of HCl dissolves one molecule of CaCO<sub>3</sub>. Therefore, the amount of consumed hydronium ions is the same of consumed limestone.

The experimental values related to the limestone consumption evaluated as molar flow rate [kmol/h] are presented in Table 7. These values are obtained considering the consumed limestone [moles] and the time required by the single experiment. The results shows that the limestone consumption is one order magnitude higher when using the ultrasounds (except for the Wolica small size fraction sample). This is directly correlated to the enhancing effect of the ultrasounds power on the sample dissolution. The highest limestone consumption is found when using the Wolica small size fraction with the use of the ultrasounds, confirming that this is the most reactive sample.

**Table 7:** Limestone consumption.

<b>sample</b>	<b>type of experiment</b>	<b>CaCO<sub>3</sub> consumption [kmol/h]</b>
Wolica Large	without US	5,2924E-06
Wolica Large	with US	1,1778E-05
Wolica Small	without US	1,0270E-05
Wolica Small	with US	1,2002E-05
Parainen Large	without US	5,6042E-06
Parainen Large	with US	1,0595E-05
Parainen Small	without US	8,1301E-06
Parainen Small	with US	1,2092E-05

The removal efficiency can be expressed through the following formula,

$$E_f = 1 - \frac{y_{SO_2,out}}{y_{SO_2,in}} \quad (4.3.1)$$

where  $y_{SO_2,out}$  and  $y_{SO_2,in}$  are respectively the composition of the stream exiting and entering the scrubber.

The molar flow balance for  $CaCO_3$  in the control volume of the scrubber gives the limestone consumption,

$$\dot{n}_{CaCO_3,in} - \dot{n}_{CaCO_3,out} = \dot{n}_{SO_2,in} E_f \quad (4.3.2)$$

with  $\dot{n}_{CaCO_3,in}$  and  $\dot{n}_{CaCO_3,out}$  the molar flows of the stream of entering and exiting limestone, and  $\dot{n}_{SO_2,in}$  the molar flow of the flue gas stream entering.

From the last equation, for a given removal efficiency and a given molar flow of entering flue gas, it is possible to compare in terms of removal efficiency, or, equivalently, in terms of limestone consumption, the samples tested in this experimental work, restating that the most reactive sample was the Wolica small size fraction.

# 5 Scale-up study

## 5.1 Power consumption for the agitation of the reaction tank

In this section a study of a simplified model of a counter-flow spray scrubber with forced oxidation was performed. This particular system was considered because it is the most commonly used in industrial applications (Kiil et al., 1998).

In a spray scrubber with forced oxidation the systems requiring up to the 90% of the total power for the operation comprise the booster fan of the inlet exhaust gas, the oxidation air blower, the ball mill for limestone grinding and the pumps for the recirculation of the slurry. The remaining 10% of the total power is needed for other pumps, for the dehydration of the slurry for the gypsum disposal and the power required for the stirring of the reaction tank.

In the previous chapter an assessment of the limestone consumption for different types of sample and size fractions was calculated, therefore the focus will be on the power required for the agitation of the slurry in the reaction tank. The power required for the agitation accounts roughly up to the 3% of the total power, so compared to the other systems is relatively low, but its assessment is still crucial to guarantee the minimum speed for the complete suspension so that there are not solid particles at the bottom of the stirred vessel (T. N. Zwietering, 1958). This precaution is necessary to avoid that the available surface for the reaction is not enough exposed to the bulk and therefore to ensure a complete use of the reagent.

The power necessary to run a given stirrer depends on the type of stirrer and the geometrical combination between the stirring tank and the stirrer. In literature the power required for the stirring has been empirically correlated to the kinematic viscosity of the liquid phase, the density of the liquid phase, the diameter of the stirrer, the diameter of the stirred reactor, the

stirring speed of the stirrer, the gravitational constant, geometric parameters related to the blade and others related to the stirrer and the tank dimensions (Pangarkar, 2015).

Traditionally this approach leads to the definition of a dimensionless parameter, the power number or Newton number for a single impeller,

$$N_p = \frac{P}{N^3 D^5 \rho_L} \quad (5.1.1)$$

where P is the power required for a single impeller, N is the speed of the impeller, D is the diameter of the impeller and  $\rho_L$  is the density of the liquid phase.

There are some differences between the stirring tank used in this experimental work and the model of this section, while other parameters have been preserved. These differences regards the type of the impeller and some approximations related the geometry of the tank.

In the considered model the following aspects related to the laboratory tank have been kept unchanged: the geometrical ratio between the diameter of the tank and the diameter of the impeller, the agitation speed and the impeller Reynold number.

This approximation was done for two main reasons: the determination of the power number for an impeller is not a trivial matter, it requires direct measures of the input power which have not been done in this work. In addition, WFGD stirring tanks are not equipped with a single blade propeller mounted on a single shaft, but they have usually multiple side entering stirrers. Therefore the power number have been estimated based on the power numbers available in the literature. Many experimental investigations have found that if the agitation of the reaction tank is sufficiently high to produce a turbulent flow, the power number reaches a constant value for a given geometry.

In particular, for the power number of a six-blade pitched-blade turbines the following correlation related to the geometry of the tank has been found (Rewatkar, Rao, & Joshi, 1990),

$$N_p = 0.653 T^{0.26} \left(\frac{T}{D}\right)^{0.11} \left(\frac{C}{T}\right)^{-0.23} n_b^{0.68} A^{1.82} \quad (5.1.2)$$

where  $T$  is the diameter of the reactor,  $D$  is the diameter of the impeller,  $C$  is the off-bottom clearance of the impeller,  $n_b$  is the number of blades and  $A$  is the impeller blade angle. All the geometrical quantities have to be expressed in m. This equation is valid for  $3 < T/D < 6$ ,  $0.125 \leq C/T \leq 0.33$ ,  $0.5 \leq A \leq 1.05$  and  $4 \leq n_b \leq 6$ .

Assuming an impeller blade angle of  $45^\circ$  and a  $C/T$  ratio of 0.125,  $N_p$  is equal to 1,425.

The impeller Reynolds number was obtained with the equation (3.1.10) and it is larger than 4000, so the turbulent flow is assured and it is possible to assume the power number constant to the calculated value.

Finally the power required for the stirring,

$$P = \rho N_p N^3 D^5 \quad (5.1.3)$$

where  $P$  is the power absorbed by a single impeller. Even though in this work it was considered the power absorbed by a single impeller, it should be noted that a reactor has usually multiple impellers, so the total power absorbed for the stirring of the reaction tank can be obtained multiplying this latter value for the number of the impellers.

## 5.2 Scaling-up criteria

Scaling-up is a way to know the main phenomena taking place in a process in order to estimate a prediction of the performance of a larger scale equipment. In applications involving solid-liquid mixing, the aim of a scale-up process is the assessment of the operating conditions at various scales preserving the same mixing yields. The behaviour of the different phases during the agitation can be observed in laboratory or pilot plant experiments realized in transparent vessels. These tests should be designed to give information regarding the level of suspension prescribed for the process, the settling velocity, the minimum suspension speed, solid-liquid mass transfer coefficient and construction materials.

Many criteria have been adopted in different research works to predict the scaling-up rule for solid mixing suspension. The main rules employed in literature are:

- constant mean dissipated energy per unit volume or unit mass,  $\varepsilon = \frac{N_p \rho_L N^3 D^5}{V}$
- constant tip speed,  $ND^n$

These two criteria are similar from a qualitative point of view since for a given system ( given  $\rho_L$  ) and a given stirrer (given  $N_p$ ), the mean dissipated energy criterion is reduced to having constant  $N^3 D^5$ .

Assuming geometrical similarities between the experimental equipment and the model, this equation has been found (Pangarkar, 2015),

$$\varepsilon \propto \text{scale factor}^{2-3b}$$

with  $b=0.85$ .

According to the last equation, the mean dissipated energy increases for values of  $b < 2/3$ , it is constant when  $b=2/3$  and it decreases when  $b > 2/3$ .

The other rule is the constant tip speed criterion and two different values has been proposed depending on the suspension condition:  $n=0.67$  for the just suspended condition and  $n=1$  for the complete suspension ( Zwietering criterion).

Another approach on constant tip speed evaluated on solid suspension in multi-impeller stirred vessels reported a value of  $n=0.93$  (Montante, Pinelli, & Magelli, 2003). According to Montante et al., 2003 , both scale-up criteria can be reduced to the expression  $ND^n$  where  $n=1$  corresponds to constant tip speed criterion,  $n=2/3$  corresponds to constant specific dissipated energy, and  $n=0.93$  as intermediate value between the two methods.

Considering a large scale reactor geometrically similar with the reactor of the model, with an impeller of a diameter of 1,32 m (so having considered an equipment 40 times larger than the small scale model), the speed of the large scale impeller was calculated with the three different criteria and then the power required for the stirring of the large scale reactor was obtained. In Figure 26 the power for the stirring of the large scale reactor is presented: while the criterion of the constant mean dissipated energy appeared to be the most demanding in terms of power required, the other two criteria are more similar.

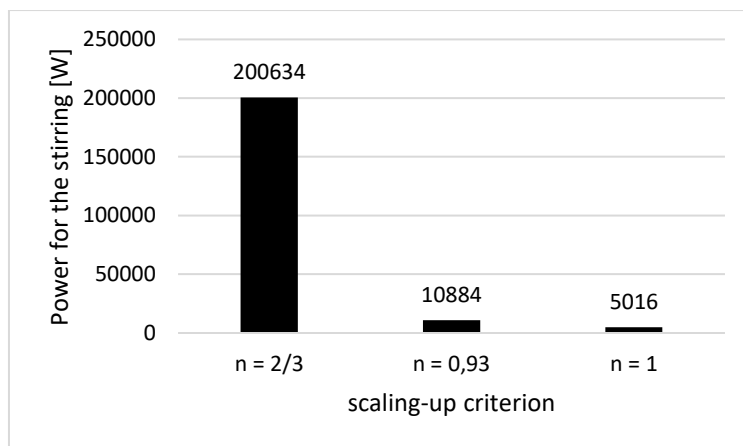


**Figure 26:** Power needed for the stirring of the large scale reactor for the three different scale-up criteria.

This variety in the final results confirms the need to further and more specific detailed investigations on small scale equipment in order to get rid of some uncertainties. Further experimental investigations could be focused on the latter two criteria, also they should try to relate the power consumption to the limestone consumption of each samples and they should include direct measures of the torque of the shaft of the stirrer of the laboratory or of the small scale equipment.

# Conclusions

A large amount of research has been devoted for the last 30 years to study limestone dissolution and it is still today a challenging topic.

The aim of this work was to study limestone dissolution through particle characterization using laser diffractometry, also taking advantage of ultrasonic power measures. The implementation of a systematic experimental procedure applied to a system with transient pH provided the specific surface area and the calculation of the limestone consumption for two different type of limestone samples. These parameters were used to calculate the total surface area of reaction, which is an important factor affecting the kinetics of a reaction. Furthermore, after the review of the main scale-up criteria adopted in literature, three criteria were chosen to perform a preliminary estimation of the power required for the stirring of a large scale reaction tank of an industrial WFGD scrubber. The diversity of the results related to the three criteria confirms the challenging nature of this subject and the need for further investigations in order to get rid of some uncertainties.

The scale-up study can be developed further:

- By direct measures of the torque of the impeller shaft of the laboratory, in order to have a more precise assessment of the settling velocity needed for particles suspension
- Considering different types of impellers and different geometrical configurations
- By including a study on a pilot plant, in order to gain a better conformity in the assessment of the involved parameters
- By relating the consumed power to the limestone consumption of each samples, in order to have an evaluation of the specific removal efficiency.

# Notation

$A$  : impeller blade angle  
 $a$  : dimensionless coefficient, Sherwood equation  
 $b$  : dimensionless constant  
 $C$  : dimensionless coefficient, Sherwood equation  
 $C$  : off-bottom clearance of the impeller  
 $C_D$  : drag coefficient  
 $D$  : impeller diameter (m)  
 $Da$  : dimensionless parameter, Damköhler number  
 $D_j$  : mass diffusivity of species  $j$  ( $m^2$ )  
 $d_p$  : particle diameter ( $\mu m$ )  
 $D_s$  : impeller diameter (m)  
 $E_a$  : apparent activation energy (kJ/mol)  
 $E_f$  : removal efficiency  
 $g$  : acceleration of gravity ( $m^2/s$ )  
 $k_l$  : pre-exponential factor ( $L/m^2s$ )  
 $k_l$  : liquid phase mass transfer coefficient (m/s)  
 $k_r$  : chemical reaction constant ( $L/m^2s$ )  
 $\dot{n}$  : molar flow (kmol/h)  
 $N$  : stirring speed (1/s)  
 $n_b$  : number of blades of the impeller  
 $N_p$  : power number  
 $P$  : power consumed in the stirring unit (W)  
 $Re$  : Reynolds number  
 $Re_p$  : Reynolds number of the particles  
 $Re_v$  : Reynolds number for the vessel

$R_g$  : universal gas constant (J/mol K)

$S$  : parameter for the Zwietering correlation

$Sc$  : Schmidt number

$Sh$  : Sherwood number

$Sh_o$  : dimensionless coefficient, Sherwood equation

$SSA$  : specific surface area (m<sup>2</sup>/g)

$T$  : reactor diameter (m)

$T_{mean}$  : reference mean temperature of the modified Arrhenius equation (K)

$u_s$  : settling velocity (m/s)

$X_{mass}$  : solid fraction (mass)

$y_{SO_2}$  : SO<sub>2</sub> composition in the stream

### **Greek letters**

$\varepsilon$  : mean dissipated energy (W/kg)

$\nu$  : kinematic viscosity of the liquid (m<sup>2</sup>/s)

$\rho_l$  : liquid density (kg/m<sup>3</sup>)

$\rho_s$  : solid density (kg/m<sup>3</sup>)

$\varphi$  : volumetric fraction of solids

# Bibliografy

- Ahlbeck, J., Engman, T., Fältén, S., & Vihma, M. (1993). A method for measuring the reactivity of absorbents for wet flue gas desulfurization. *Chemical Engineering Science*, 48(20), 3479–3484. [https://doi.org/10.1016/0009-2509\(93\)85003-8](https://doi.org/10.1016/0009-2509(93)85003-8)
- Ahlbeck, J., Engman, T., Fältén, S., & Vihma, M. (1995). Measuring the reactivity of limestone for wet flue-gas desulfurization. *Chemical Engineering Science*, 50(7), 1081–1089. [https://doi.org/10.1016/0009-2509\(94\)00482-7](https://doi.org/10.1016/0009-2509(94)00482-7)
- Al Omari, M. M. H., Rashid, I. S., Qinna, N. A., Jaber, A. M., & Badwan, A. A. (2016). *Calcium Carbonate. Profiles of Drug Substances, Excipients and Related Methodology* (1st ed., Vol. 41). Elsevier Inc. <https://doi.org/10.1016/bs.podrm.2015.11.003>
- Altun, N. E. (2014). Assessment of marble waste utilization as an alternative sorbent to limestone for SO<sub>2</sub> control. *Fuel Processing Technology*, 128, 461–470. <https://doi.org/10.1016/j.fuproc.2014.08.009>
- Baukal, C. E. (2003). *Industrial Combustion Pollution and Control*. CRC Press. Retrieved from [https://books.google.it/books?id=-S7JYclfS\\_4C](https://books.google.it/books?id=-S7JYclfS_4C)
- Bird, R. B., Stewart, W. E., & Lightfoot, E. N. (2002). *Transport phenomena Second Edition* (Vol. 1). <https://doi.org/10.1002/aic.690070245>
- Bjerle, I., & Rochelle, G. T. (1984). Limestone dissolution from a plane surface. *Chemical Engineering Science*, 39(1), 183–185. [https://doi.org/10.1016/0009-2509\(84\)80151-7](https://doi.org/10.1016/0009-2509(84)80151-7)
- Carletti, C., Grénman, H., De Blasio, C., Mäkilä, E., Salonen, J., Murzin, D. Y., ... Westerlund, T. (2016). Revisiting the dissolution kinetics of limestone - experimental analysis and modeling. *Journal of Chemical Technology and Biotechnology*, 91(5), 1517–1531.

<https://doi.org/10.1002/jctb.4750>

- De Blasio, C., Carletti, C., Lundell, A., Visuri, V. V., Kokkonen, T., Westerlund, T., ... Järvinen, M. (2016). Employing a step-wise titration method under semi-slow reaction regime for evaluating the reactivity of limestone and dolomite in acidic environment. *Minerals Engineering*, *86*, 43–58. <https://doi.org/10.1016/j.mineng.2015.11.011>
- Eden, B. D., & Luckas, M. (1998). A Heat and Mass Transfer Model for the Simulation of the Wet Limestone Flue Gas Scrubbing Process 2 The Wet Limestone Flue Gas Scrubbing. *Chemical Engineering Journal*, *21*(1), 56–60.
- EEA. (2014). Sulphur dioxide ( SO<sub>2</sub> ) emissions. Retrieved from <https://www.eea.europa.eu/data-and-maps/indicators/eea-32-sulphur-dioxide-so2-emissions-1/assessment-3>
- F.J.Gutiérrez Ortiz, F.Vidal, P.Ollero, L.Salvador, V.Cortés, A. G. (2006). Pilot-Plant Technical Assessment of Wet Flue Gas Desulfurization Using Limestone, 1466–1477.
- Franco, A., & Diaz, A. R. (2009). The future challenges for “clean coal technologies”: Joining efficiency increase and pollutant emission control. *Energy*, *34*(3), 348–354. <https://doi.org/10.1016/j.energy.2008.09.012>
- Frandsen, J. B. W., Kiil, S., & Johnsson, J. E. (2001). Optimisation of a wet FGD pilot plant using fine limestone and organic acids. *Chemical Engineering Science*, *56*(10), 3275–3287. [https://doi.org/10.1016/S0009-2509\(01\)00010-0](https://doi.org/10.1016/S0009-2509(01)00010-0)
- Guelli U Souza, S. M. A., Santos, F. B. F., Ulson de Souza, A. A., & Vidal Barrero, F. (2010). Limestone dissolution in flue gas desulfurization-experimental and numerical study. *Journal of Chemical Technology & Biotechnology*, *85*(9), 1208–1214. <https://doi.org/10.1002/jctb.2418>
- Holdich, R. (2002). Fundamentals of particle technology. *Fundamentals of Particle Technology*, *6*, 6–20. [https://doi.org/10.1016/S0958-2118\(08\)70183-6](https://doi.org/10.1016/S0958-2118(08)70183-6)

- Hrastel, I., Gerbec, M., & Stergaršek, A. (2007). Technology Optimization of Wet Flue Gas Desulfurization Process, (2), 220–233. <https://doi.org/10.1002/ceat.200600314>
- Ibrahim, S., Jasnin, S. N., Wong, S. D., & Baker, I. F. (2012). Zwieterings equation for the suspension of porous particles and the use of curved blade impellers. *International Journal of Chemical Engineering*, 2012. <https://doi.org/10.1155/2012/749760>
- IEA. (2015). Energy and Climate Change. *World Energy Outlook Special Report*, 1–200. <https://doi.org/10.1038/479267b>
- J. Welty, Gregory L. Rorrer, and D. G. F. (1970). *Fundamentals of momentum, heat and mass transfer*. *International Journal of Heat and Mass Transfer* (Vol. 13). [https://doi.org/10.1016/0017-9310\(70\)90063-3](https://doi.org/10.1016/0017-9310(70)90063-3)
- Kaminski, J. (2003). Technologies and costs of SO<sub>2</sub> -emissions reduction for the energy sector, 75, 165–172. [https://doi.org/10.1016/S0306-2619\(03\)00029-1](https://doi.org/10.1016/S0306-2619(03)00029-1)
- Kiil, S., Michelsen, M. L., & Dam-Johansen, K. (1998). Experimental Investigation and Modeling of a Wet Flue Gas Desulfurization Pilot Plant, 5885(97), 2792–2806.
- Kitto, J. B., & Stultz, S. C. (2005). *Steam its generation and use*. <https://doi.org/10.1007/978-1-4614-4310-0>
- Lancia, A., Musmarra, D., & Pepe, F. (1997). Mass Transfer between a Fixed Bed of Limestone Particles and Acid Solutions. *Industrial and Engineering Chemistry Research*, 36(9), 3859–3865.
- Levenspiel. (1999). *Chemical Reaction Engineering*. *Chemical Engineering Science* (Vol. 19). [https://doi.org/10.1016/0009-2509\(64\)85017-X](https://doi.org/10.1016/0009-2509(64)85017-X)
- Liu, S., & Xiao, W. (2006). New wet flue gas desulfurization process using granular limestone and organic acid additives. *International Journal of Chemical Reactor Engineering*, 4(1).
- Lund, K., Fogler, H. S., & McCune, C. C. (1977). Acidization-I. The dissolution of dolomite in hydrochloric acid. *Chemical Engineering Science*, 28(3), 691–700.

[https://doi.org/10.1016/0009-2509\(77\)80003-1](https://doi.org/10.1016/0009-2509(77)80003-1)

Montante, G., Pinelli, D., & Magelli, F. (2003). Scale-up criteria for the solids distribution in slurry reactors stirred with multiple impellers. *Chemical Engineering Science*, 58(23–24), 5363–5372. <https://doi.org/10.1016/j.ces.2003.09.021>

Olausson, S., Wallin, M., & Bjerle, I. (1993). A model for the absorption of sulphur dioxide into a limestone slurry. *The Chemical Engineering Journal*, 51(2), 99–108. [https://doi.org/10.1016/0300-9467\(93\)80016-H](https://doi.org/10.1016/0300-9467(93)80016-H)

Pangarkar, V. G. (2015). *Design of multiphase reactors*.

Paul, E. L., Atiemo-Obeng, V. A., & Kresta, S. M. (2004). *Rotor-Stator Mixing Devices. HANDBOOK OF INDUSTRIAL MIXING Science and practice*. <https://doi.org/10.1002/0471451452>

Pepe, F. (2001). Dissolution of finely ground limestone particles in acidic solutions. *Industrial and Engineering Chemistry Research*, 40(23), 5378–5385. <https://doi.org/10.1021/ie001119j>

Plummer, L., Wigley, T., & Parkhurs, D. (1978). The kinetics of calcite dissolution in CO<sub>2</sub>-water systems at 5° to 60° and 0.0 to 1.0 atm CO<sub>2</sub>.

Rewatkar, V. B., Rao, R., & Joshi, J. B. (1990). Power Consumption in Mechanically Agitated Contactors Using Pitched Bladed Turbine Impellers. *Chemical Engineering Communications*, 88(1), 69–90. <https://doi.org/10.1080/00986449008940548>

Rhodes, M. (2008). *Introduction to Particle Technology. Chemical Engineering and Processing (Vol. 7)*. <https://doi.org/10.1002/9780470727102>

Roddy, D. (2010). *Advanced Power Plant Materials, Design and Technology*. Elsevier Science. Retrieved from <https://books.google.it/books?id=b5FwAgAAQBAJ>

Sargent & Lundy LLC. (2003). *Wet Flue Gas Desulfurization Technology Evaluation*, (January).

- Shafiee, S., & Topal, E. (2009). When will fossil fuel reserves be diminished? *Energy Policy*, 37(1), 181–189. <https://doi.org/10.1016/j.enpol.2008.08.016>
- Shih, S. M., Lin, J. P., & Shiau, G. Y. (2000). Dissolution rates of limestones of different sources. *Journal of Hazardous Materials*, 79(1–2), 159–171. [https://doi.org/10.1016/S0304-3894\(00\)00253-3](https://doi.org/10.1016/S0304-3894(00)00253-3)
- Siagi, Z. O., & Mbarawa, M. (2009). Dissolution rate of South African calcium-based materials at constant pH. *Journal of Hazardous Materials*, 163(2–3), 678–682. <https://doi.org/10.1016/j.jhazmat.2008.07.014>
- Sjöberg, E. L., & Rickard, D. (1983). The influence of experimental design on the rate of calcite dissolution. *Geochimica et Cosmochimica Acta*, 47(12), 2281–2285. [https://doi.org/10.1016/0016-7037\(83\)90051-0](https://doi.org/10.1016/0016-7037(83)90051-0)
- Sjöberg, E. L., & Rickard, D. T. (1985). The effect of added dissolved calcium on calcite dissolution kinetics in aqueous solutions at 25°C. *Chemical Geology*, 49(4), 405–413. [https://doi.org/10.1016/0009-2541\(85\)90002-6](https://doi.org/10.1016/0009-2541(85)90002-6)
- Sloss, L. (2011). Legislation in the European Union and the impact on existing plant. Retrieved from <https://www.iea.org/media/workshops/2011/platformrussia/Sloss.pdf>
- Srivastava, R. K., & Jozewicz, W. (2001). Flue gas desulfurization: The state of the art. *Journal of the Air and Waste Management Association*, 51(12), 1676–1688. <https://doi.org/10.1080/10473289.2001.10464387>
- T. N. Zwietering. (1958). Suspending of solid particles in liquid by agitators. *Chemical Engineering Science*, 8, 244–253.
- Toprac, & Rochelle. (1982). Limestone Dissolution in Stock Gas Desulfurization. *Environmental Program*, 1(1).
- Ukawa, N., Takashina, T., Shinoda, N., & Shimizu, T. (1993). Effects of particle size distribution on limestone dissolution in wet FGD process applications. *Environmental Progress*,

12(3), 238–242. <https://doi.org/10.1002/ep.670120314>

Williams, B. B., Gidley, J. L., Guin, J. A., Schechter, R. S., Gidley, J. L., Guin, J. A., ... Williams, B. B. (1970). Characterization of Liquid-Solid Reactions: Hydrochloric Acid-Calcium Carbonate Reaction. *Industrial and Engineering Chemistry Fundamentals*, 9(4), 589–596. <https://doi.org/10.1021/i160036a011>

Zhong, Y., Gao, X., Huo, W., Luo, Z. yang, Ni, M. jiang, & Cen, K. fa. (2008). A model for performance optimization of wet flue gas desulfurization systems of power plants. *Fuel Processing Technology*, 89(11), 1025–1032. <https://doi.org/10.1016/j.fuproc.2008.04.004>

# Appendices

## Acid consumption calculation

### Data sheet

- 1) Copy in the SSA measurements table with the time and the SSA the data taken from the exported Malvern excel SSA measurements.
- 2) Copy the pH measurements exported from the software HI92500. You find them in the pH504 sheet.
- 3) Plot the pH evolution for every step.
- 4) Look at the time column of the SSA table and try to find the closest values of the time in the pH tables. Highlight them because you need the pH values for the acid consumption evaluation.

<b>Sample</b>	Wolica Large
<b>Sample mass [g]</b>	2,0056
<b>HCl [mL]</b>	1
<b>Stirrer speed [rpm]</b>	2300

### Malvern measurements data

<b>Average background</b>	
time	16:19:25
SSA [g/m <sup>2</sup> ]	9,224292908

### SSA measurements

<b>Step1 measurements</b>		SSA
	time	[g/m <sup>2</sup> ]
t1	16:21:32	9,2384586
t2	16:23:48	9,3174523
t3	16:24:31	9,3028347
t4	16:25:14	9,323893
t5	16:25:57	9,3458478
t6	16:26:41	9,3075216
t7	16:27:24	9,35799
t8	16:28:07	9,3447289
t9	16:28:50	9,3538332
t10	16:29:33	9,3366497
t11	16:30:16	9,336958
t12	16:30:59	9,3802745
t13	16:31:43	9,3049622
t14	16:32:26	9,3619855

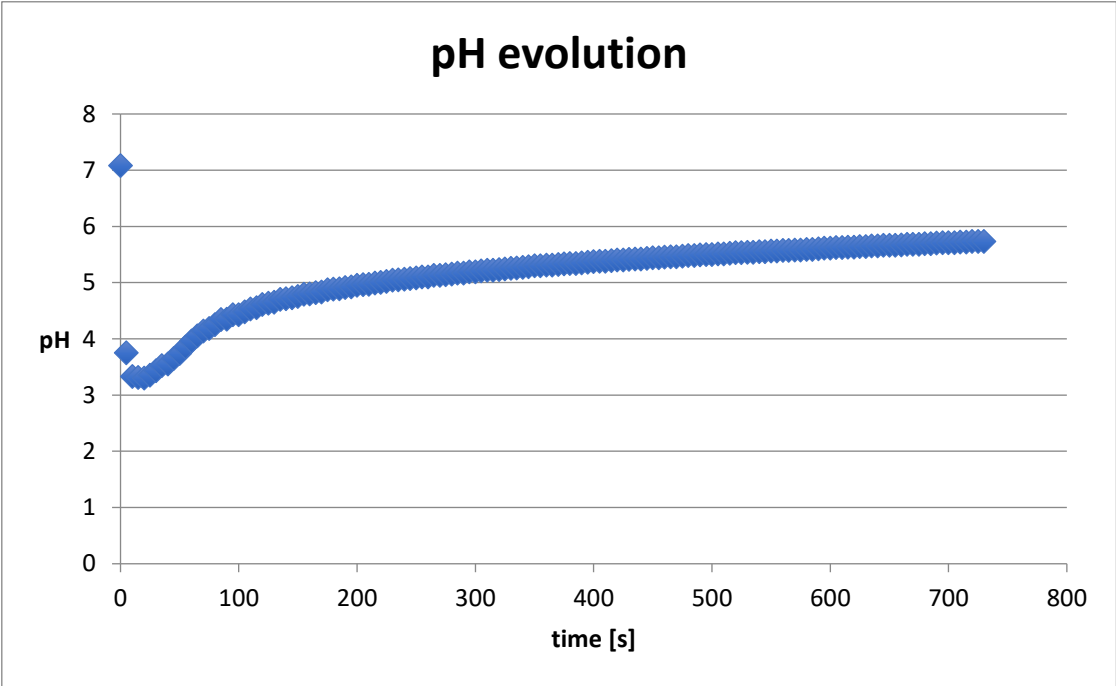
## pH measures

First step of measurements		
time	time [s]	pH
16:20:49	0	7,08
16:20:54	5	3,75
16:20:59	10	3,33
16:21:04	15	3,31
16:21:09	20	3,3
16:21:14	25	3,35
16:21:19	30	3,43
16:21:24	35	3,52
16:21:29	40	3,55
16:21:34	45	3,65
16:21:39	50	3,74
16:21:44	55	3,85
16:21:49	60	3,96
16:21:54	65	4,05
16:21:59	70	4,14
16:22:04	75	4,18
16:22:09	80	4,25
16:22:14	85	4,34
16:22:19	90	4,35
16:22:24	95	4,43
16:22:29	100	4,43
16:22:34	105	4,48
16:22:39	110	4,53
16:22:44	115	4,55
16:22:49	120	4,61
16:22:54	125	4,63
16:22:59	130	4,65
16:23:04	135	4,7
16:23:09	140	4,71
16:23:14	145	4,73
16:23:19	150	4,75
16:23:24	155	4,79
16:23:29	160	4,8
16:23:34	165	4,82
16:23:39	170	4,83
16:23:45	175	4,87
16:23:50	180	4,88
16:23:55	185	4,89
16:24:00	190	4,91
16:24:05	195	4,92

16:24:10	200	4,95
16:24:15	205	4,96
16:24:20	210	4,97
16:24:25	215	4,99
16:24:30	220	5
16:24:35	225	5,02
16:24:40	230	5,04
16:24:45	235	5,05
16:24:50	240	5,06
16:24:55	245	5,07
16:25:00	250	5,08
16:25:05	255	5,1
16:25:10	260	5,1
16:25:15	265	5,13
16:25:20	270	5,13
16:25:25	275	5,14
16:25:30	280	5,15
16:25:35	285	5,17
16:25:40	290	5,17
16:25:45	295	5,19
16:25:50	300	5,19
16:25:55	305	5,21
16:26:00	310	5,22
16:26:05	315	5,22
16:26:10	320	5,23
16:26:15	325	5,24
16:26:20	330	5,25
16:26:25	335	5,26
16:26:30	340	5,27
16:26:35	345	5,28
16:26:40	350	5,3
16:26:46	355	5,3
16:26:51	360	5,31
16:26:56	365	5,31
16:27:01	370	5,32
16:27:06	375	5,33
16:27:11	380	5,34
16:27:16	385	5,34
16:27:21	390	5,35
16:27:26	395	5,36
16:27:31	400	5,37
16:27:36	405	5,38
16:27:41	410	5,38
16:27:46	415	5,39
16:27:51	420	5,4
16:27:56	425	5,4
16:28:01	430	5,41
16:28:06	435	5,42
16:28:11	440	5,42
16:28:16	445	5,43

16:28:21	450	5,44
16:28:26	455	5,44
16:28:31	460	5,45
16:28:36	465	5,46
16:28:41	470	5,46
16:28:46	475	5,47
16:28:51	480	5,48
16:28:56	485	5,48
16:29:01	490	5,49
16:29:06	495	5,5
16:29:11	500	5,5
16:29:16	505	5,51
16:29:21	510	5,51
16:29:26	515	5,52
16:29:32	520	5,53
16:29:37	525	5,53
16:29:42	530	5,54
16:29:47	535	5,54
16:29:52	540	5,55
16:29:57	545	5,55
16:30:02	550	5,56
16:30:07	555	5,56
16:30:12	560	5,57
16:30:17	565	5,57
16:30:22	570	5,58
16:30:27	575	5,58
16:30:32	580	5,59
16:30:37	585	5,59
16:30:42	590	5,6
16:30:47	595	5,61
16:30:52	600	5,61
16:30:57	605	5,62
16:31:02	610	5,62
16:31:07	615	5,63
16:31:12	620	5,63
16:31:17	625	5,64
16:31:22	630	5,64
16:31:27	635	5,65
16:31:32	640	5,65
16:31:37	645	5,66
16:31:42	650	5,66
16:31:47	655	5,66
16:31:52	660	5,67
16:31:58	665	5,68
16:32:03	670	5,68
16:32:08	675	5,68
16:32:13	680	5,69
16:32:18	685	5,69
16:32:23	690	5,7
16:32:28	695	5,71

16:32:33	700	5,71
16:32:38	705	5,71
16:32:43	710	5,72
16:32:48	715	5,72
16:32:53	720	5,73
16:32:58	725	5,73
16:33:03	730	5,73



## Acid consumption sheet: step by step procedure

### 1) Table 1

copy from the first step of measurements (in the data sheet) the initial records columns, it should be the first 80 seconds ( more or less). Put a zero in the time cell and recalculate the time column.

### 2) Table 2:

copy from the data sheet the step1 measurements table, add a column for the pH, and copy the pH values chosen from the first sheet, except for the first row pH cell (pink cell).

### 3) Table 3:

copy the first row of the table 1, except for the pH cell (blue cell). Look at the time t1 of the table 2 and in the table 2 look for the record right after the time t1. Copy the related row and the following rows in the table 3.

### 4) Table 4:

copy from Step1 measurements table of the data sheet, copy the background pH in the brown cell, drag all the cells until the pH00 cell (blue cell).

bg [H<sup>+</sup>]: from the pH definition  $\text{pH} = -\text{Log}_{10}(\text{H}^+) \rightarrow [\text{H}^+] = (1/10)^{\text{pH}}$

actual bg H<sup>+</sup> mol in 0.5 l: the actual content of [H<sup>+</sup>] in 0.5 l of solution

total H<sup>+</sup> in 0.5 sol: sum of the [H<sup>+</sup>] contained in the water and the [H<sup>+</sup>] from HCl. Block the HCl value.

[H<sup>+</sup>]: it's valid just for 1l of solution, and the definition of pH is valid for 1 l of solution, so every time I need to use the formula from the definition of pH, I have to divide/multiply for 2.

pH00: theoretical pH directly calculated from the pH definition.

Leave the other cells empty for now.

### 5) Table 5:

copy the first row of the table 3, and the time  $t_1$  of the first row of the table 2. Calculate how many seconds are from the time zero to time  $t_1$ . Put this value in the time cell of the second row. Leave the pH column empty.

### 6) Interpolation plot:

plot the pH vs time columns from table 5. Make an interpolation, using the excel function 'trendline', choosing a polynomial equation, putting the theoretical pH as intersection with the y axis and assuring that  $R^2 > 0.99$  (which means the fitting is high).

### 7) Table 5:

In the table 5, copy the trendline equation in the pH cell (pink cell), substituting the time (s) of the second row. In this way, you can obtain the pH corresponding to the first  $t_1$  measure.

### 8) Table 4

Copy the pH value found with the interpolation in the first row of the table 4, and then copy the pH column from the table 2.

H<sup>+</sup> moles in 1 l solution: pH definition → H<sup>+</sup> moles in 1 l of solution and drag.

Total H<sup>+</sup> in the solution: half of the H<sup>+</sup> in 1 l and drag.

Consumed HCl moles: difference between the total H<sup>+</sup> when the HCl was added (block the cell) and the amount of H<sup>+</sup> in the  $t_1$  time. Drag.

Consumed CaCO<sub>3</sub> moles: the same number of moles of HCl ( see the CaCO<sub>3</sub> dissolution reaction).

Consumed CaCO<sub>3</sub> mass: product of the CaCO<sub>3</sub> moles and the molar weight.

Remaining CaCO<sub>3</sub>: difference between the initial sample mass (block this value, because we always consider the difference between the initial mass and the consumed at every  $t_n$  measurements) and the consumed CaCO<sub>3</sub> mass in  $t_1$ . Drag.

SSA: copy the column from the table 2. Drag.

TSA: product of the SSA and the remaining  $\text{CaCO}_3$  mass. Drag.

### Second step of measurements and further steps.

#### 9) Table 6:

Copy the background pH value of the first row of the table 1 in the background pH cell (brown cell).

Background  $[\text{H}^+]$  concentration: from the pH definition.

Actual background  $[\text{H}^+]$  concentration: half of the previous one.

Consumed HCl moles: difference between the total bg  $\text{H}^+$  in 0.5 l of solution from the table 4 of the previous step and the actual backgr. concentration.

Consumed  $\text{CaCO}_3$  mass: product between the consumed  $\text{CaCO}_3$  moles and the molar weight.

Remaining mass: difference between the initial sample mass and the consumed  $\text{CaCO}_3$  mass.

From the third step, the remaining mass is the difference between the remaining mass of the previous step and the the consumed  $\text{CaCO}_3$  mass of the current step.

Use the same procedure seen before for the following calculations.

**Table 1**

First measure_t1		
time	time [s]	pH
16:20:49	0	7,08
16:20:54	5	3,75
16:20:59	10	3,33
16:21:04	15	3,31
16:21:09	20	3,3
16:21:14	25	3,35
16:21:19	30	3,43
16:21:24	35	3,52
16:21:29	40	3,55
16:21:34	45	3,65
16:21:39	50	3,74
16:21:44	55	3,85
16:21:49	60	3,96

16:21:54	65	4,05
16:21:59	70	4,14
16:22:04	75	4,18
16:22:09	80	4,25

**Table 2**

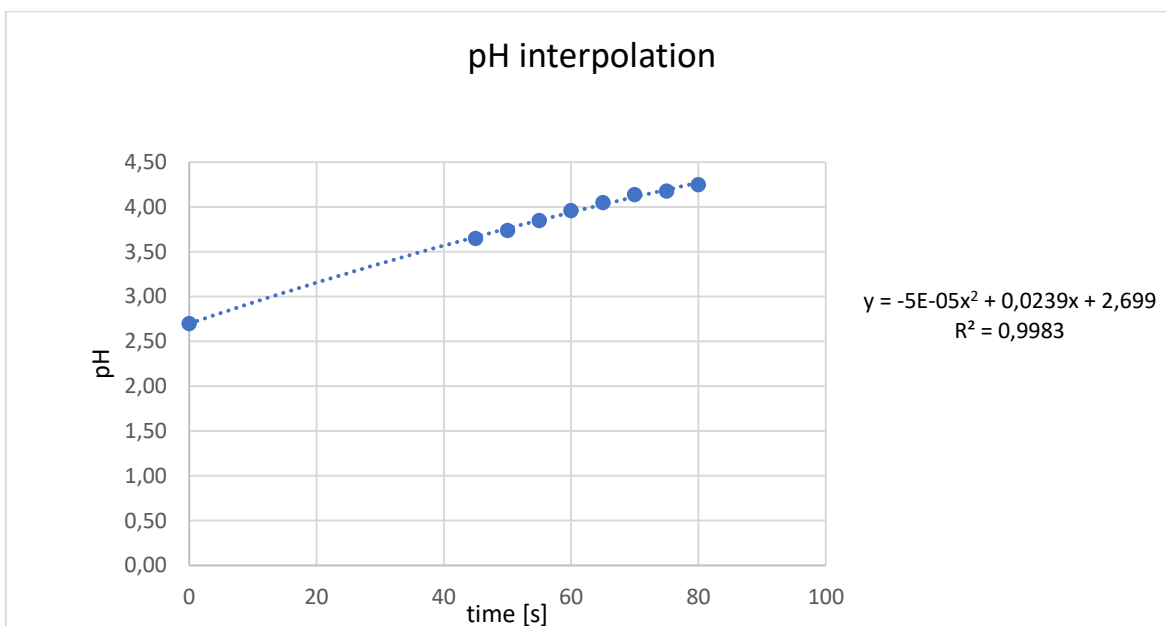
Step measurements			
	time	SSA [g/m <sup>2</sup> ]	pH
t1	16:21:32	9,24	3,63
t2	16:23:48	9,32	4,88
t3	16:24:31	9,30	5
t4	16:25:14	9,32	5,13
t5	16:25:57	9,35	5,21
t6	16:26:41	9,31	5,3
t7	16:27:24	9,36	5,36
t8	16:28:07	9,34	5,42
t9	16:28:50	9,35	5,48
t10	16:29:33	9,34	5,53
t11	16:30:16	9,34	5,57
t12	16:30:59	9,38	5,62
t13	16:31:43	9,30	5,66
t14	16:32:26	9,36	5,71

**Table 3**

pH table		
time	time [s]	pH
16:20:49	0	2,70
16:21:34	45	3,65
16:21:39	50	3,74
16:21:44	55	3,85
16:21:49	60	3,96
16:21:54	65	4,05
16:21:59	70	4,14
16:22:04	75	4,18
16:22:09	80	4,25

**Table 5**

time	time [s]	pH
16:20:49	0	2,70
16:21:32	43	3,63

**Table 6****Second step of measurements\_t1 measure**

background pH	5,80
background [H <sup>+</sup> ] concentration	1,58E-06
actual background [H <sup>+</sup> ] concentration in 0.5 l of solution	7,92E-07
consumed HCl moles	0,0009992
consumed CaCO <sub>3</sub> moles	0,0009992
consumed CaCO <sub>3</sub> mass	0,100015
remaining mass [g]	1,9055852